Title

Sbf/MTMR13 coordinates PI(3)P and Rab21 regulation in endocytic control of cellular remodeling.

Journal

Molecular biology of the cell, 23(14)

ISSN

1059-1524

Authors

Jean, Steve
Cox, Sarah
Schmidt, Eric J
et al.

Publication Date

2012-07-01

DOI

10.1091/mbc.e12-05-0375

Peer reviewed

Sbf/MTMR13 coordinates PI(3)P and Rab21 regulation in endocytic control of cellular remodeling

Steve Jean[a], Sarah Cox[a], Eric J. Schmidt[b], Fred L. Robinson[b], and Amy Kiger[a]
[a]Division of Biological Sciences, University of California, San Diego, La Jolla, CA 92093-0380; [b]Department of Neurology, Oregon Health and Science University, Portland, OR 97239

ABSTRACT **Cells rely on the coordinated regulation of lipid phosphoinositides and Rab GTPases to define membrane compartment fates along distinct trafficking routes. The family of disease-related myotubularin (MTM) phosphoinositide phosphatases includes catalytically inactive members, or pseudophosphatases, with poorly understood functions. We found that *Drosophila* MTM pseudophosphatase Sbf coordinates both phosphatidylinositol 3-phosphate (PI(3)P) turnover and Rab21 GTPase activation in an endosomal pathway that controls macrophage remodeling. Sbf dynamically interacts with class II phosphatidylinositol 3-kinase and stably recruits Mtm to promote turnover of a PI(3)P subpool essential for endosomal trafficking. Sbf also functions as a guanine nucleotide exchange factor that promotes Rab21 GTPase activation associated with PI(3)P endosomes. Of importance, Sbf, Mtm, and Rab21 function together, along with Rab11-mediated endosomal trafficking, to control macrophage protrusion formation. This identifies Sbf as a critical coordinator of PI(3)P and Rab21 regulation, which specifies an endosomal pathway and cortical control.**

Monitoring Editor
Francis A. Barr
University of Liverpool

Received: May 15, 2012
Accepted: May 22, 2012

INTRODUCTION

Remodeling of the cell surface through membrane trafficking is important for changes in cell shape and function. The correct combinations of phosphoinositides, phosphorylated forms of phosphatidylinositol, and members of the Rab GTPase family are crucial to control dynamic membrane identities between intersecting trafficking pathways in the cell (Di Paolo and De Camilli, 2006; Grosshans *et al.*, 2006). Early endosomal membranes under the direction of phosphatidylinositol 3-phosphate (PI(3)P) and Rab5 GTPase are sites of protein sorting that can lead to cargo recycling back to the plasma membrane or to lysosomal degradation. Thus endocytosis provides a means for rapid changes in cell shape and surface protein composition, activity, and organization (Grant and Donaldson, 2009).

PI(3)P mediates membrane recruitment of effectors with specific roles in endocytosis or autophagy (Lindmo and Stenmark, 2006), making the coordinated regulation of PI(3)P critical. PI(3)P regulation is best understood through its synthesis by two classes of phosphatidylinositol 3-kinases (PI3-kinases). The conserved class III PI3-kinase Vps34 is recruited to the Vps15/p150 adaptor within distinct protein complexes (Backer, 2008). The metazoan-restricted class II PI3-kinase (PI3KC2; MacDougall *et al.*, 1995) is implicated in cortical functions (MacDougall *et al.*, 1995; Maffucci *et al.*, 2005; Falasca *et al.*, 2007; Srivastava *et al.*, 2009; Velichkova *et al.*, 2010) and can interact with clathrin and signaling adaptors at the plasma membrane (Gaidarov *et al.*, 2001; Wheeler and Domin, 2001), although mechanisms of PI3KC2 functions are unclear. Conversely, PI(3)P down-regulation occurs with endosomal maturation, both by conversion to phosphatidylinositol 3,5 bisphosphate ($PI(3,5)P_2$; Gary *et al.*, 1998) and by depletion upon endosomal membrane exit (efflux), potentially through kinase inactivation, sorting, and/or dephosphorylation (Egami and Araki, 2008; Velichkova *et al.*, 2010). However, the cellular demands and mechanisms that govern down-regulation of PI(3)P subpools are less well understood.

This article was published online ahead of print in MBoC in Press (http://www.molbiolcell.org/cgi/doi/10.1091/mbc.E12-05-0375) on May 30, 2012.

Address correspondence to: Amy Kiger (akiger@ucsd.edu).

Abbreviations used: CA, constitutive active; coIP, coimmunoprecipitation; DENN, differentially expressed in neoplastic versus normal cells; DN, dominant negative; F-actin, filamentous actin; FRAP, fluorescence recovery after photobleaching; GEF, guanine nucleotide exchange factor; IP, immunoprecipitation; MTM, myotubularin; *mtm*, *Drosophila myotubularin* gene; PI3-kinase, phosphatidylinositol 3-kinase; PI3KC2, class II PI3-kinase; PI(3)P, phosphatidylinositol 3-phosphate; UAS, upstream activating sequence; WT, wild type.

The large family of disease-relevant myotubularin (MTM) phosphoinositide phosphatases are selective for PI(3)P and PI(3,5)P_2 (Laporte *et al.*, 1996; Bolino *et al.*, 2000; Taylor *et al.*, 2000; Berger *et al.*, 2002; Kim *et al.*, 2002). MTMs have been identified with endosomal roles that impact the trafficking of specific surface receptors and adhesion proteins, or cortical remodeling (Kim *et al.*, 2002; Tsujita *et al.*, 2004; Cao *et al.*, 2008; Lee *et al.*, 2010; Silhankova *et al.*, 2010; Velichkova *et al.*, 2010; Ribeiro *et al.*, 2011). MTM-specific functions suggest a need for differential regulation toward distinct phosphoinositide pools. Half of the MTM family members encode for catalytically inactive phosphatases ("pseudophosphatases"; Laporte *et al.*, 1998; Robinson and Dixon, 2006). MTM pseudophosphatases have been found to share mutant phenotypes and form direct protein interactions with MTM catalytic phosphatases (Firestein *et al.*, 2002; Azzedine *et al.*, 2003; Kim *et al.*, 2003; Senderek *et al.*, 2003; Dang *et al.*, 2004; Robinson and Dixon, 2005; Robinson *et al.*, 2008; Berger *et al.*, 2006; Lorenzo *et al.*, 2006; Tersar *et al.*, 2007; Silhankova *et al.*, 2010). Although speculated to serve as phosphatase adaptors, the contributions of MTM pseudophosphatases to phosphoinositide homeostasis in cell functions have not been tested.

Like phosphoinositides, Rab GTPases are under dynamic regulation to mediate membrane trafficking. Opposing functions of guanine nucleotide exchange factors (GEFs) and GTPase-activating proteins (GAPs) direct localized Rab activity (Behnia and Munro, 2005). The importance of Rab GTPase and phosphoinositide combinations is illustrated at endosomes, where codependent Rab5 and Vps34 activities coordinate the recruitment of effectors via coincidence detection of Rab5-GTP and PI(3)P (Behnia and Munro, 2005; Di Paolo and De Camilli, 2006). Although phosphoinositides and Rabs are often functionally coupled, surprisingly few mechanisms for their coordinated regulation are established. Of interest, differentially expressed in neoplastic versus normal cells (DENN)-domain-containing proteins, including MTMR5/MTMR13, were recently shown to exhibit Rab GEF activity (Yoshimura *et al.*, 2010), raising the possibility of pseudophosphatase roles in simultaneous phosphoinositide and Rab regulation.

Immune cell surveillance requires rapid changes in cell shape, including extension–retraction of cell protrusions. Previously, we showed that *Drosophila* Mtm phosphatase, the single homologue of human MTM1/MTMR2/MTMR1, regulates a PI3KC2-dependent PI(3)P pool to mediate macrophage protrusion formation and recruitment to wounds (Velichkova *et al.*, 2010). Here we show that the mechanism of cellular remodeling relies on Sbf, an MTMR13/MTMR5 pseudophosphatase, and its dual roles in phosphoinositide and Rab GTPase regulation.

RESULTS

Sbf and *mtm* are codependent in macrophages for cell protrusions and animal viability

We recently described specific immune cell roles for *mtm* phosphatase in hemocytes, or insect macrophages, for cell remodeling, recruitment to wounds, and animal viability (Velichkova *et al.*, 2010), highlighting the importance of a PI(3)P pool balance for normal macrophage function. To explore unknown roles for MTM pseudophosphatases in PI(3)P regulation and functions, we investigated a macrophage requirement for any of the three coexpressed *Drosophila* MTM pseudophosphatases (Sbf, CG14411, CG5026; Supplemental Figure S1A). We found that only *Sbf*, encoding the single homologue of human MTMR5/MTMR13 (Figure 1, A and B), was required for fly adult viability when depleted in macrophages (Supplemental Figure S1, B–I; with either of two RNA interference [RNAi] hairpins). Fly viability was rescued with coexpression of a wild-type (WT) *mCherry:Sbf* cDNA (Supplemental Figure S1C), indicating the specificity of *Sbf* knockdown. The lack of a complete rescue can be explained by a high efficiency of RNAi, as suggested by endogenous Sbf depletion and undetectable mCherry:Sbf fluorescence despite restored essential *Sbf* function (Supplemental Figure S1, F–I). These results suggest that *Sbf* may act specifically in the same processes as *mtm* that are important for macrophage function.

Macrophages exhibit a dynamic cell cortex that is important for immune surveillance functions. When isolated from the animal, larval macrophages spread flat and extend and retract prominent radial cell protrusions rich in filamentous actin (F-actin; Figure 1C). Given an *mtm* role that promotes cell protrusion formation to mediate immune cell recruitment, we examined whether *Sbf* shares a similar cortical function. *Sbf*-depleted macrophages spread but failed to extend F-actin–rich protrusions (Figure 1, D–F, Supplemental Figure S1, J–M, and Supplemental Video S1), similar in severity to the *mtm*-null allele (Velichkova *et al.*, 2010). In contrast, overexpression of *Sbf* exhibited an opposite phenotype of an increased number of protrusions per cell when expressed alone or in combination with *mtm* (Figure 1, G–I, and Supplemental Figure S1, N–Q). Thus both *Sbf* and *mtm* are necessary and sufficient to establish the appropriate balance of F-actin protrusions in macrophages.

The formation of cellular protrusions provides a clear and relevant cellular read-out of *Sbf* and *mtm* function. To assess whether *Sbf* and *mtm* act in the same pathway, we performed epistasis analysis by testing whether depletion of one could block the formation of excess protrusions driven by expression of the other. *Sbf* depletion completely blocked *mtm*-induced protrusions, and, moreover, most cells lacked any protrusions (Figure 1, H′, H″, and J), indicating that ectopic *mtm* could not overcome the requirement for *Sbf*. The corequirement for *Sbf* is unlikely to be simply due to effects on Mtm protein level, since mCherry:Mtm fluorescence was still detectable when expressed in affected *Sbf* RNAi cells yet was undetectable despite an ability to rescue *mtm* RNAi cells (Figure 1, K and L). Likewise, *mtm* was required for *Sbf*-induced excess protrusions (Figure 1, I′, I″, and M), although the macrophages exhibited a new phenotype of unextended F-actin fibers (Figure 1I′), suggesting that *Sbf* might possess additional functions independent of *mtm* (see later discussion). Taken together, these results show that *Sbf* and *mtm* functions are codependent in cell protrusion formation.

Sbf pseudophosphatase recruits Mtm into a stable interaction

The foregoing results identified a corequirement for *Sbf* and *mtm* in the control of cell shape. To test whether *Sbf* and *mtm* share functions mediated through their protein interactions, we performed coimmunoprecipitation (coIP) and phosphatase activity assays. Sbf and Mtm could be isolated in a protein complex (Figure 2A and Figure 4A later in the paper for converse coIP), as in mammals (Kim *et al.*, 2003). Expressed Sbf was able to coimmunoprecipitate an endogenous protein with Mtm molecular weight and phosphatase activity (Figure 2B). We observed no significant difference in Mtm phosphatase activity toward both of its known substrates, PI(3)P and PI(3,5)P_2, when expressed either with or without Sbf (Figure 2C). This suggests that an *Sbf* role required for *mtm* function in macrophages is likely to localize and/or locally stabilize Mtm activity.

To better understand an *Sbf* role in cortical remodeling, we assessed Sbf localization. In macrophages, Sbf was found on intracellular puncta and enriched along the plasma membrane and nearly undetectable in *Sbf*-depleted cells (Figure 2, D–F). Time-lapse microscopy indicated that mCherry:Sbf puncta were dynamic

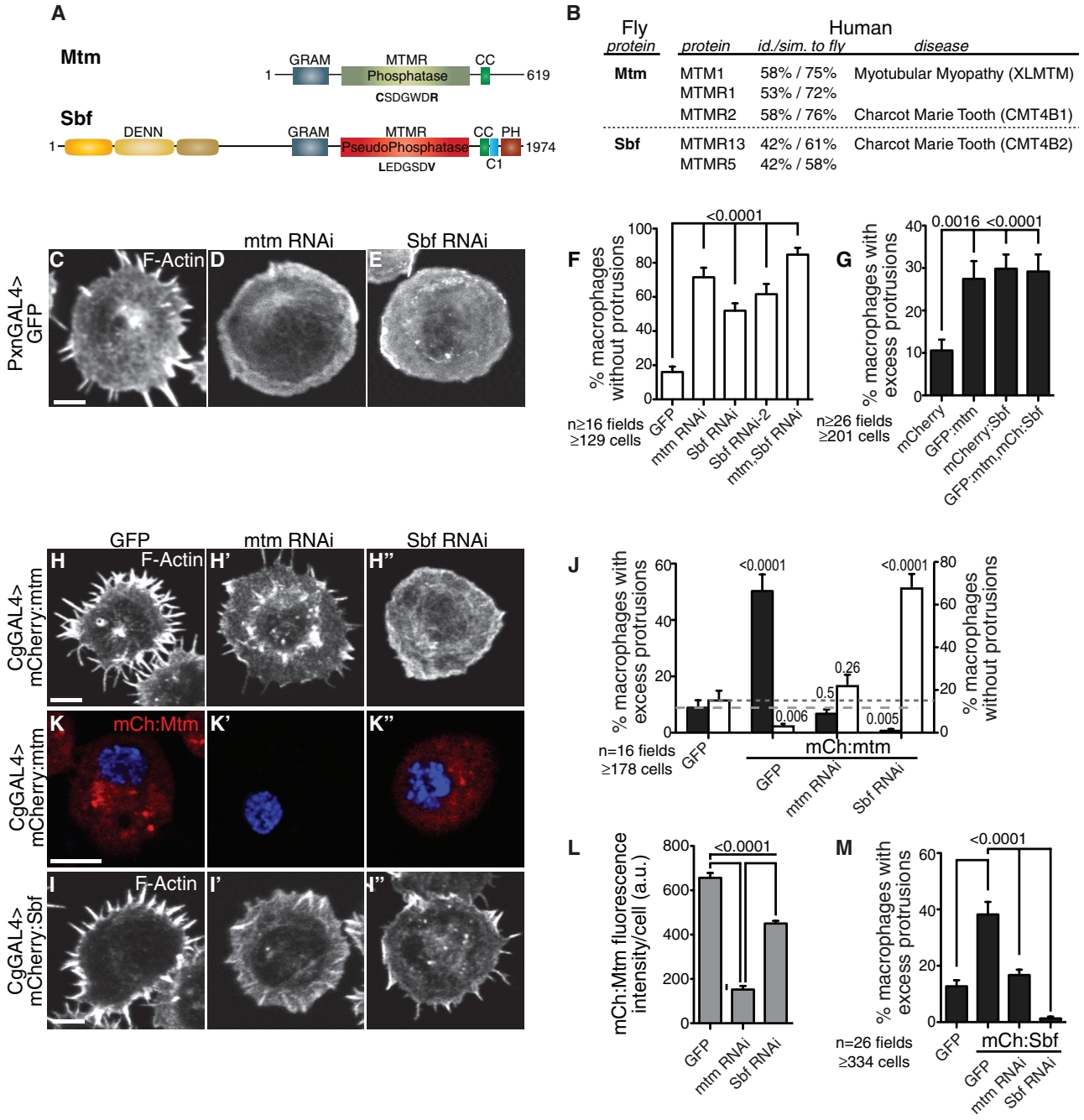

FIGURE 1: *Sbf* and *mtm* are corequired for macrophage protrusions. (A) *Drosophila* Mtm phosphatase and Sbf pseudophosphatase. (B) Mtm and Sbf human homologues and associated diseases. (C–E, H–I″) F-Actin in primary macrophages. (C) Normal number and extent of radial protrusions in control cell. Protrusions are missing upon Pxn-GAL4 macrophage–targeted (D) *mtm* RNAi or (E) *Sbf* RNAi. (F) Percentage of macrophages without cell protrusions upon RNAi. (G) Percentage of cells with excess protrusions upon wild-type cDNA expression. (H) *mtm* or (I) *Sbf* induces excess macrophage protrusions, suppressed by (H′, I′) *mtm* or (H″, I″) *Sbf* coRNAi. (J) Percentage of control and *mtm*-overexpressing cells with excess (black) and loss (white) of protrusions. (K) mCherry:Mtm (red) in control, (K′) *mtm* RNAi, and (K″) *Sbf* RNAi cells. (L) mCherry:Mtm fluorescence intensity per cell. (M) Percentage of control and *Sbf*-overexpressing cells with excess protrusions, +SEM. Bars, 5 μm.

(Supplemental Video S2). In contrast to the cortical Sbf localization, green fluorescent protein (GFP):Mtm when expressed alone was mainly cytoplasmic and weakly detectable on intracellular rings (Figure 2G). However, coexpression of mCherry:Sbf with GFP:Mtm (Figure 2, H–H‴) dramatically shifted Mtm from a mostly diffuse to a striking cortical and vesicular distribution that colocalized with Sbf (Figure 2H′; 0.56 ± 0.02 Pearson's correlation), suggesting that Sbf recruits Mtm into a stable protein complex at membranes.

To explore the ability of Sbf to control Mtm localization, we performed fluorescence recovery after photobleaching (FRAP). Recovery curves for bleached regions of GFP:Mtm were rapidly restored

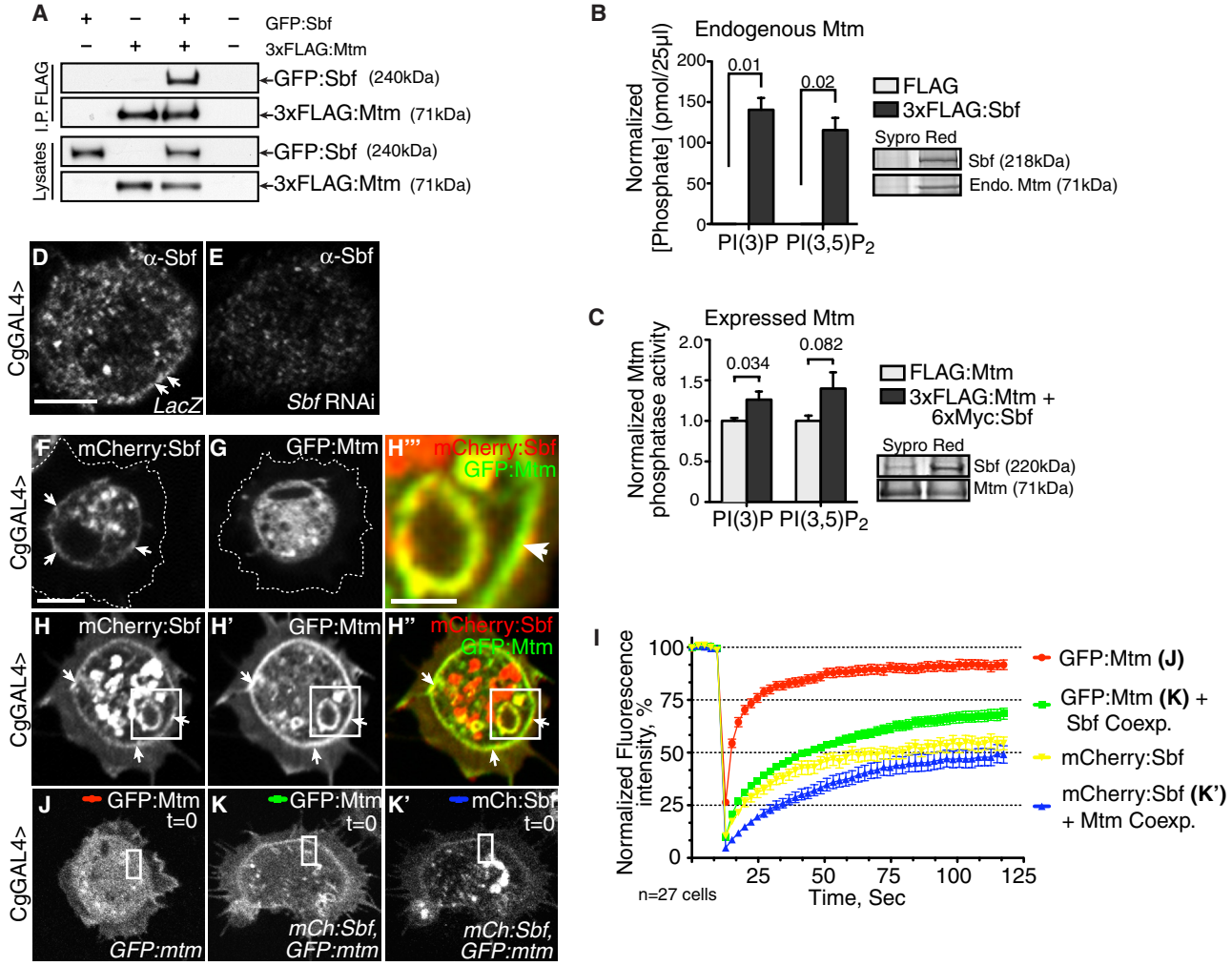

FIGURE 2: Sbf recruits Mtm into a stable complex at membranes. (A) Mtm interacts with Sbf in Kc_{167} cells. IP of 3xFLAG:Mtm and GFP immunoblot of GFP:Sbf. (B, C) Phosphatase activity toward PI(3)P and PI(3,5)P_2. (B) FLAG (white) and 3xFLAG:Sbf (gray) IP-released phosphate concentration normalized to protein level. (C) 3xFLAG:Mtm IP, with or without Sbf coexpression. Fold activity normalized to condition with Mtm expressed alone, +SEM. Sypro Red stain shows a similar amount of IP. (D–K′) Primary macrophages. (D) Endogenous Sbf localization at the plasma membrane of the cell body (arrows) and internal puncta. (E) Sbf immunostaining in *Sbf* RNAi-depleted cells; note the absence of membrane staining. (F) Live cell imaging of mCherry:Sbf, with a similar pattern as endogenous protein. (G) GFP:Mtm localizes mainly to cytoplasm and few internal foci. (H–H‴) When coexpressed, (H) mCherry:Sbf recruits (H′) GFP:Mtm to the cell cortex and internal rings, and both exhibit stabilized levels. (H″) Merge and (H‴) zoom of box. (I) Time course of recovery shown as normalized fluorescence intensity for GFP:Mtm (red) or mCherry:Sbf (yellow) expressed alone or in combination (Mtm, green; Sbf, blue), ±SEM. (J–K′) Representative bleached regions at 0 s for data in I. Cg-GAL4. Bars, 5 µm, except H‴, 1.25 µm.

to near prebleach levels (85.2 ± 2.0% mean intensity at 46 s), indicating that Mtm is highly mobile and diffuses rapidly in cells (Figure 2, I and J). In contrast, mCherry:Sbf exhibited delayed and only partial recovery (43.5 ± 3.2% mean intensity at 46 s), revealing that more than half of the Sbf was in an immobile or more stabilized fraction (Figure 2I). In agreement with Sbf recruitment of Mtm protein, there was a marked decrease in Mtm FRAP recovery when coexpressed with Sbf (Figure 2, I and K). There was also a slight decrease in Sbf recovery curves when coexpressed with Mtm (Figure 2, I and K′). These FRAP results clearly demonstrate that Sbf, an MTM pseudophosphatase, modifies and stabilizes the localization of Mtm phosphatase within a shared protein complex. Given that Mtm catalytic activity is required for macrophage remodeling, we propose that Sbf acts to membrane recruit an Mtm phosphatase activity required for protrusion extension.

An Sbf role in cellular remodeling depends on class II Pi3K68D kinase activity

The functional codependence between *Sbf* and *mtm* suggests that Sbf might control phosphoinositide regulation and function. To test this, we first explored a relationship between *Sbf* and the class II PI3-kinase *Pi3K68D* in the formation of cell protrusions. Codepletion of *Sbf* and *Pi3K68D* restored normal protrusion number (Figure 3, A–C). This suggests that Pi3K68D is responsible for synthesis of a phosphoinositide pool that is either the target of the Sbf–Mtm phosphatase complex or has an antagonistic function. To further test this significance, we looked at the in vivo distribution of a population of adherent macrophages normally dispersed evenly along the larval body wall (Supplemental Figure S2, A and B), correlating with an *mtm*-dependent ability for macrophage recruitment to epidermal wounds (Velichkova *et al.*, 2010). In accordance with the loss of cell

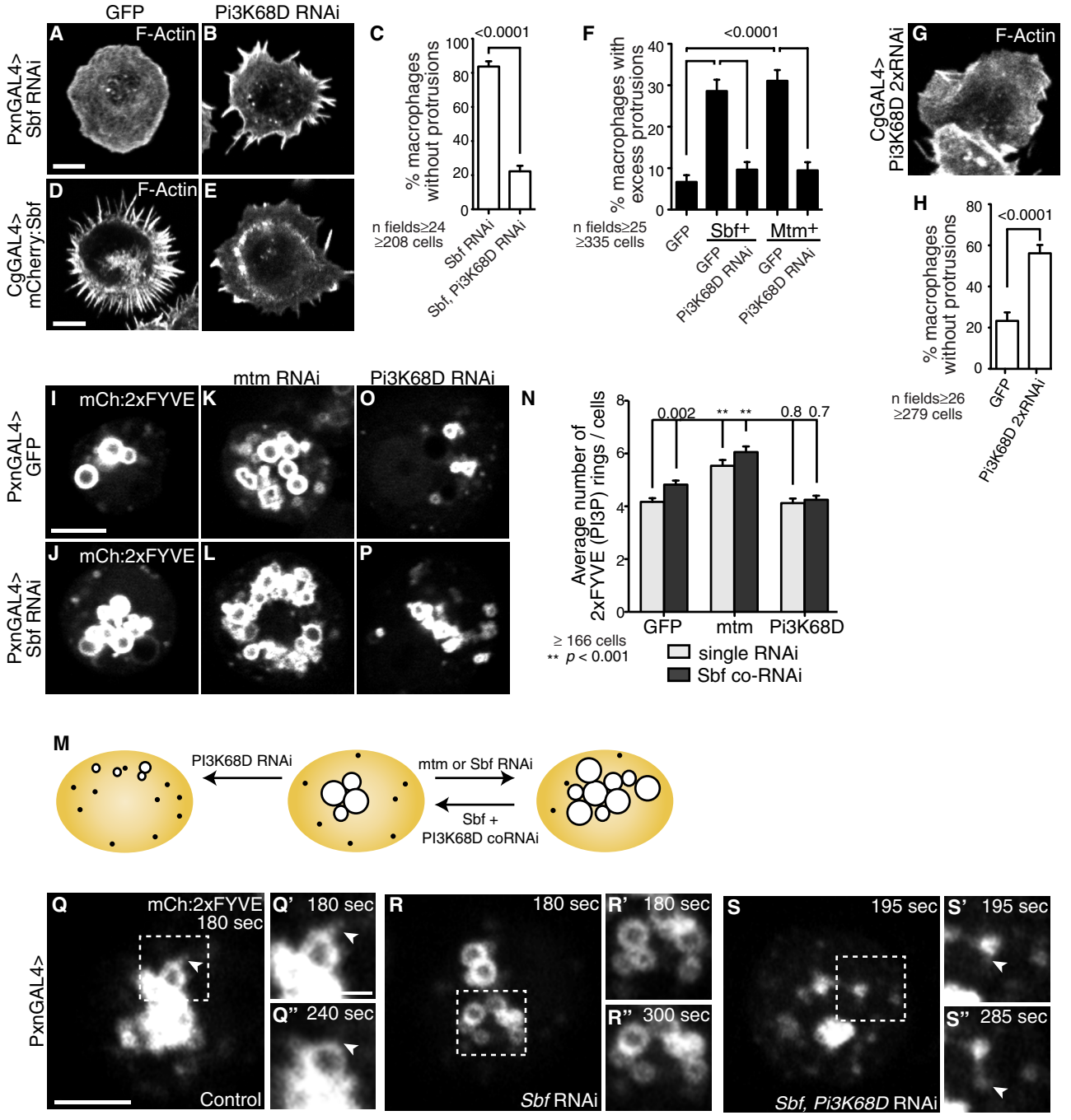

FIGURE 3: *Pi3K68D*-dependent *Sbf* functions in PI(3)P turnover, endosomal membrane exit, and macrophage protrusions. (A,B, D, E, G) F-Actin in primary macrophages. (A) Lack of protrusions with macrophage-targeted *Sbf* RNAi. (B) Rescue of normal radial protrusions with *Sbf*, *Pi3K68D* codepletion. (C) Percentage of cells without protrusions in *Sbf* RNAi or *Pi3K68D* codepleted cells; +SEM. (D) *Sbf*-induced excess protrusions, suppressed by (E) *Pi3K68D* codepletion. (F) Percentage of macrophages with excess protrusions upon *Sbf* or *mtm* cDNA expression, suppressed by *Pi3K68D* RNAi; +SEM. (G) Loss of cell protrusions with severe *Pi3K68D* depletion, using two copies of RNAi hairpin and strong Cg-GAL4 driver. (H) Percentage of macrophages without cell protrusions upon *Pi3K68D* knockdown; +SEM. (I–L, O–P) mCherry:2xFYVE detection of PI(3)P in single macrophage. (I) Normal PI(3)P distribution on several rings. (J) Accumulation of PI(3)P-containing rings with *Sbf* or (K) *mtm* RNAi, (L) enhanced by *Sbf* and *mtm* coRNAi. (M) Cartoon of PI(3)P-containing membranes observed (rings and vesicles) and quantified in control and knockdown conditions. (N) Number of PI(3)P-containing rings with visible lumen per cell; +SEM; Pxn-GAL4. (O) Partial depletion of PI(3)P with *Pi3K68D* RNAi. (P) Suppressed accumulation of PI(3)P with *Sbf* and *Pi3K68D* coRNAi. (Q–S) Still images of mCherry:2xFYVE dynamics from Supplemental Video S3. Zooms are shown of depicted regions at specified times (seconds). (Q–Q″) Control cells exhibit dynamic membrane tubules at PI(3)P-containing compartments (arrowheads). (R–R″) With *Sbf* RNAi, tubulation events were rarely observed. (S–S″) *Sbf* and *Pi3K68D* coRNAi restored the frequency of tubulation. Bars, 5 μm, except 2.5 μm in crops.

protrusions, *Sbf* and *mtm* knockdown resulted in a clumped and uneven distribution of macrophages in intact larvae (Supplemental Figure S2, C–E). Codepletion of *Pi3K68D* and *Sbf* restored the normal macrophage distribution and, of importance, suppressed fly lethality (Supplemental Figure S2, F–H). Macrophage number and phagocytic ability were unaffected in all conditions (Supplemental Figure S2, I and J). Taken together, these results demonstrate an interaction between *Sbf* and *Pi3K68D* in macrophage remodeling that is significant to macrophage distribution in vivo and likely impacts immune surveillance or developmental tissue remodeling roles essential for animal viability.

If *Sbf* and *mtm* functions reflect a requirement for a PI(3)P phosphorylation–dephosphorylation sequence at successive sites, then *Pi3K68D* function for synthesis of this pool also would be required for protrusion formation. Alternatively, if depletion of this PI(3)P pool is simply permissive, then loss of *Pi3K68D* function would instead lead to formation of excess protrusions. We found that codepletion of *Pi3K68D* was able to revert the formation of *Sbf*- or *mtm*-induced excess protrusions (Figure 3, D–F, and Supplemental Figure S2, K and L). Consistent with this suppression, a requirement for *Pi3K68D* in cell protrusion formation was revealed with severe *Pi3K68D* knockdown (Figure 3, G and H). Loss of *Pi3K68D* function did not alter Sbf or Mtm protein levels and, moreover, stabilized their colocalization (Supplemental Figure S2, M–O), suggesting that the cell protrusion defect was unlikely simply due to loss of Sbf–Mtm function. These results support the former model, suggesting a mechanism in which a Pi3K68D-dependent PI(3)P pool is subsequently a target of Sbf–Mtm. Taken together, these results demonstrate that both the normal and Sbf-induced protrusions depend on a phosphoinositide phosphorylation-dephosphorylation sequence regulated by Pi3K68D, Mtm and Sbf (see model, Supplemental Figure S3A).

Sbf regulates a Pi3K68D-dependent PI(3)P pool and endosomal membrane efflux

To test Sbf function in PI(3)P regulation, we assessed effects of *Sbf* knockdown on 2xFYVE localization as an indicator of PI(3)P distribution, previously shown to correlate with *mtm*-dependent PI(3)P levels (Velichkova *et al.*, 2010). In wild-type macrophages, PI(3)P is detected both enriched at endosomal membrane rings with obvious lumens and more weakly at small, motile vesicles (Velichkova *et al.*, 2010). Consistent with a normal Sbf role to promote Mtm-mediated PI(3)P turnover, both *Sbf* and *mtm* RNAi led to a similar increase in the number of PI(3)P-enriched rings, as well as the amount of combined size and number of PI(3)P-containing membranes (Figure 3, I–N, and Supplemental Figure S3B). In contrast, codepletion of *Sbf* and *Pi3K68D* restored the PI(3)P membranes to normal (Figure 3, M–P, and Supplemental Figure S3B), suggesting that Pi3K68D kinase activity is required for the PI(3)P accumulation. Together these results show that *Sbf* function affects a *Pi3K68D/mtm*-coregulated PI(3)P pool, with consequences both for amount and characteristics of PI(3)P-containing membranes.

PI(3)P is known to recruit effectors involved in endosomal sorting, maturation, and membrane fusion, whereas PI(3)P turnover promotes membrane exit. Using time-lapse microscopy to monitor the dynamics of PI(3)P-containing compartments, we found that tubulation events indicative of exiting membrane normally seen in control cells were infrequent in *Sbf*-depleted cells (Figure 3, Q and R). The PI(3)P membrane dynamics was rescued by *Pi3K68D* and *Sbf* codepletion (Figure 3S and Supplemental Video S3). As the first demonstration of a requirement for an MTM pseudophosphatase in phosphoinositide regulation, this shows that Sbf is critical for Mtm dephosphorylation of a PI(3)P pool that promotes endosomal membrane exit, or efflux.

Sbf and Pi3K68D interact on cell membranes

The foregoing results indicate that *Sbf* functionally interacts with both *mtm* and *Pi3K68D*. Mtm family members were shown to interact in a Vps34 kinase–MTM phosphatase complex through the adaptor Vps15 (Cao *et al.*, 2007, 2008). We asked whether Sbf could harbor such an adaptor role to complex both Pi3K68D and Mtm to promote coordinated functions. In coIP experiments from cell cultures with low levels of protein expression (see *Materials and Methods*), we found that Sbf interacts with both Mtm and Pi3K68D (Figure 4A). To corroborate the novel Sbf/Pi3K68D interaction, we performed coIP on endogenous proteins using newly generated specific antibodies (Figures S1E and S4A). Again, an Sbf/Pi3K68D interaction was detected with coIP of both endogenous proteins (Figure 4, B and C), confirming that Sbf and Pi3K68D are part of a common protein complex.

Pi3K68D was brought down by Sbf whether Mtm was coexpressed or not (Figure 4A), and in the converse coIP, Pi3K68D interacted with Mtm only when Sbf was coexpressed (Figure 4D, compare lanes 4 and 7). This suggests that the Pi3K68D–Sbf interaction is not through Mtm but that a tripartite complex can exist. Mtm IP could bring down Pi3K68D in the absence of Sbf coexpression (Supplemental Figure S4B), suggesting that Mtm can interact with the kinase, perhaps via endogenous Sbf. We were unable to map an interaction site between Sbf and Pi3K68D using truncation constructs, pointing potentially to multiple sites of interaction or to indirect interactions in a multiprotein complex. Given the complex interactions, we asked whether interactions between Sbf and Pi3K68D alter Mtm phosphatase activity. Mtm activity for PI(3)P showed only a minor decrease when coexpressed with Pi3K68D (Supplemental Figure S4C), suggesting that Pi3K68D expression does not interfere with Mtm phosphatase activity per se. Together these data suggest that Sbf can bridge Pi3K68D and Mtm in an active tripartite complex.

To determine what might distinguish the different enzyme interactions, we fractionated cells to find where the Sbf/Mtm and Sbf/Pi3K68D interactions occur. We identified that Sbf/Mtm interact both in membrane and cytoplasmic fractions. In contrast, the Sbf/Pi3K68D binding was only observed in the membrane fraction (Figure 4E), suggesting a transient or weak Sbf and Pi3K68D protein interaction at, or corecruitment to, a common membrane. In accordance with this, we observed by video microscopy under conditions of normal macrophage protrusions and cell function a transient colocalization between mCherry:Sbf and Pi3K68D:GFP motile particles (Supplemental Figure S4D and Supplemental Video S4). Of interest, levels and localization of expressed Pi3K68D were diminished in *Sbf*-depleted cells (Figure 4, F and G), consistent with an Sbf scaffolding role in Pi3K68D regulation.

Conserved MTMR13 and PI3KC2α interaction in mammals

MTMR13 was shown in mammals to have essential functions in Schwann cells for proper neuronal conductance underlying mutant association with Charcot–Marie–Tooth disease (Azzedine *et al.*, 2003; Senderek *et al.*, 2003; Tersar *et al.*, 2007; Robinson *et al.*, 2008). To assess the broader relevance of Sbf and Pi3K68D interactions discovered in flies, we asked whether MTMR13 also associates with class II PI3-kinase in mouse. Highlighting the importance of such an interaction, we found MTMR13 and PI3KC2α coIP from mouse brain (Figure 4H). Detection of PI3KC2α interaction with MTMR13, along with the previously described MTMR13–MTMR2 interaction (Robinson and Dixon, 2005), suggests conservation of a

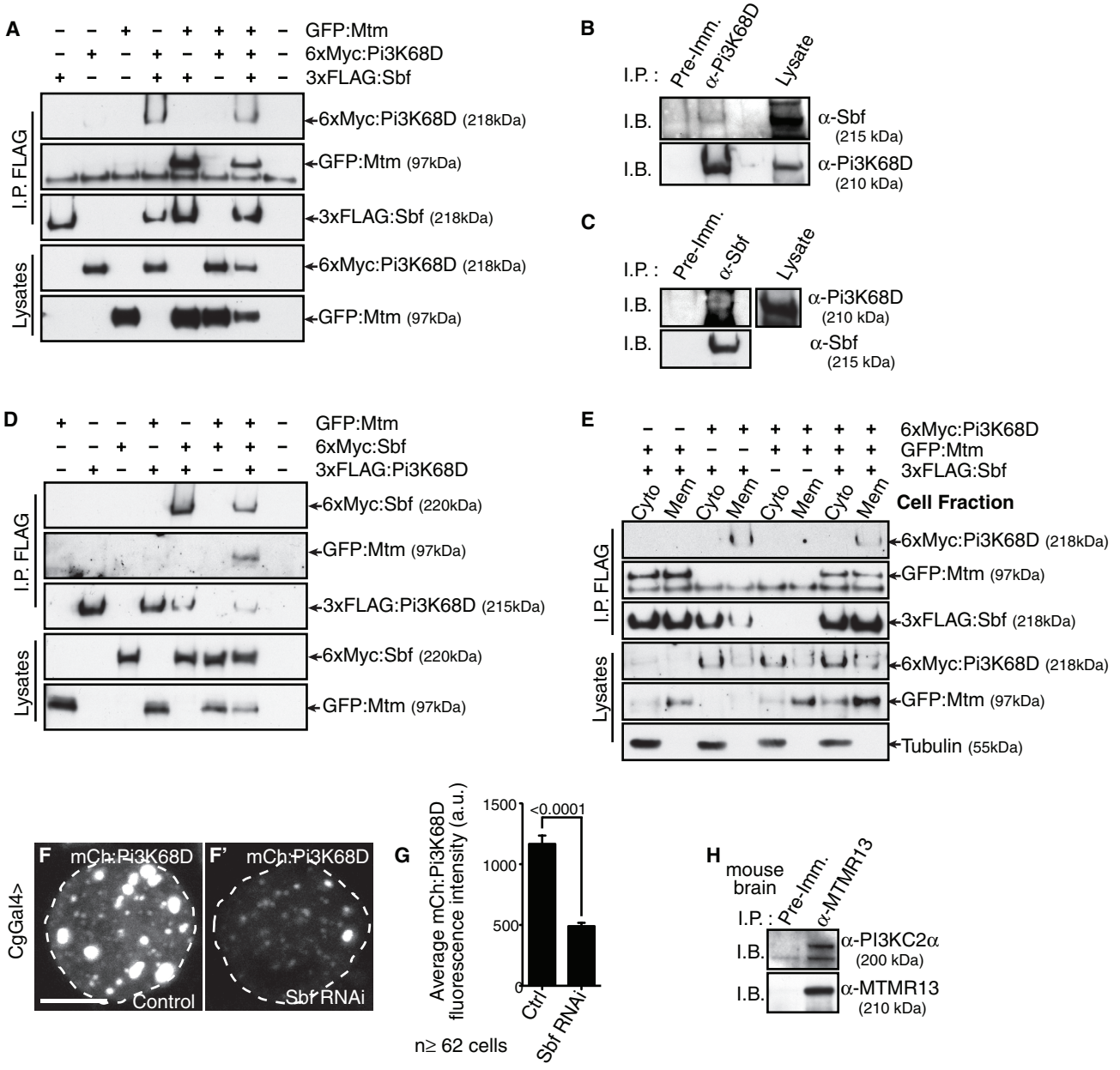

FIGURE 4: Sbf is part of a conserved protein complex comprising Mtm and Pi3K68D. (A–E) Sbf interacts with Mtm and Pi3K68D in Kc_{167} cells. (A) IP 3xFLAG:Sbf analyzed by immunoblot for coexpressed GFP:Mtm and 6xMyc:Pi3K68D. (B, C) Endogenous Sbf and Pi3K68D interact. (B) Anti-Pi3K68D coIP of endogenous Sbf. (C) Anti-Sbf coIP of endogenous Pi3K68D. (D) Pi3K68D interacts with Mtm only in the presence of Sbf expression. IP 3xFLAG:Pi3K68D and immunoblot of coexpressed GFP:Mtm and 6xMyc:Sbf. (E) Sbf interacts with Pi3K68D preferentially in cell membrane fraction. IP 3xFLAG:Sbf from crude protein membrane (Mem) or cytoplasmic (Cyto) fractions analyzed by immunoblot of coexpressed GFP:Mtm and 6xMyc:Pi3K68D. (F) mCherry:Pi3K68D in control and (F') *Sbf*-depleted macrophages. (G) mCherry:Pi3K68D fluorescence intensity per cell; +SEM. (H) MTM pseudophosphatase and class II PI3-kinase interaction is conserved in mammals. From mouse whole-brain extract, anti-MTMR13 (Ab116) coIP of endogenous PI3KC2α. Bar, 5 μm.

Pi3K68D/Sbf/Mtm pathway in mammals and potential implication of PI3KC2α in Charcot–Marie–Tooth disease.

Sbf interacts with Rab21 and Rab11 GTPases associated with endosomes

The foregoing results point to a role for an Sbf–Mtm complex in the regulation of PI(3)P and membrane dynamics, which in turn could affect cargo trafficking. We reasoned that a phosphatase activity could promote membrane exit from PI(3)P-containing endosomes, for example, in trafficking to recycling endosomes. PI(3)P is enriched on early endosomal membranes with Rab5 GTPase. The Rab5 subfamily includes Rab21 (66% similarity; Zhang *et al.*, 2007a), which in mammals has been implicated in endocytic uptake and recycling functions (Simpson *et al.*, 2004; Pellinen and Ivaska, 2006; Egami and Araki, 2008; Mai *et al.*, 2011). To address sites of Sbf function, we investigated Sbf association with Rab GTPases that specify

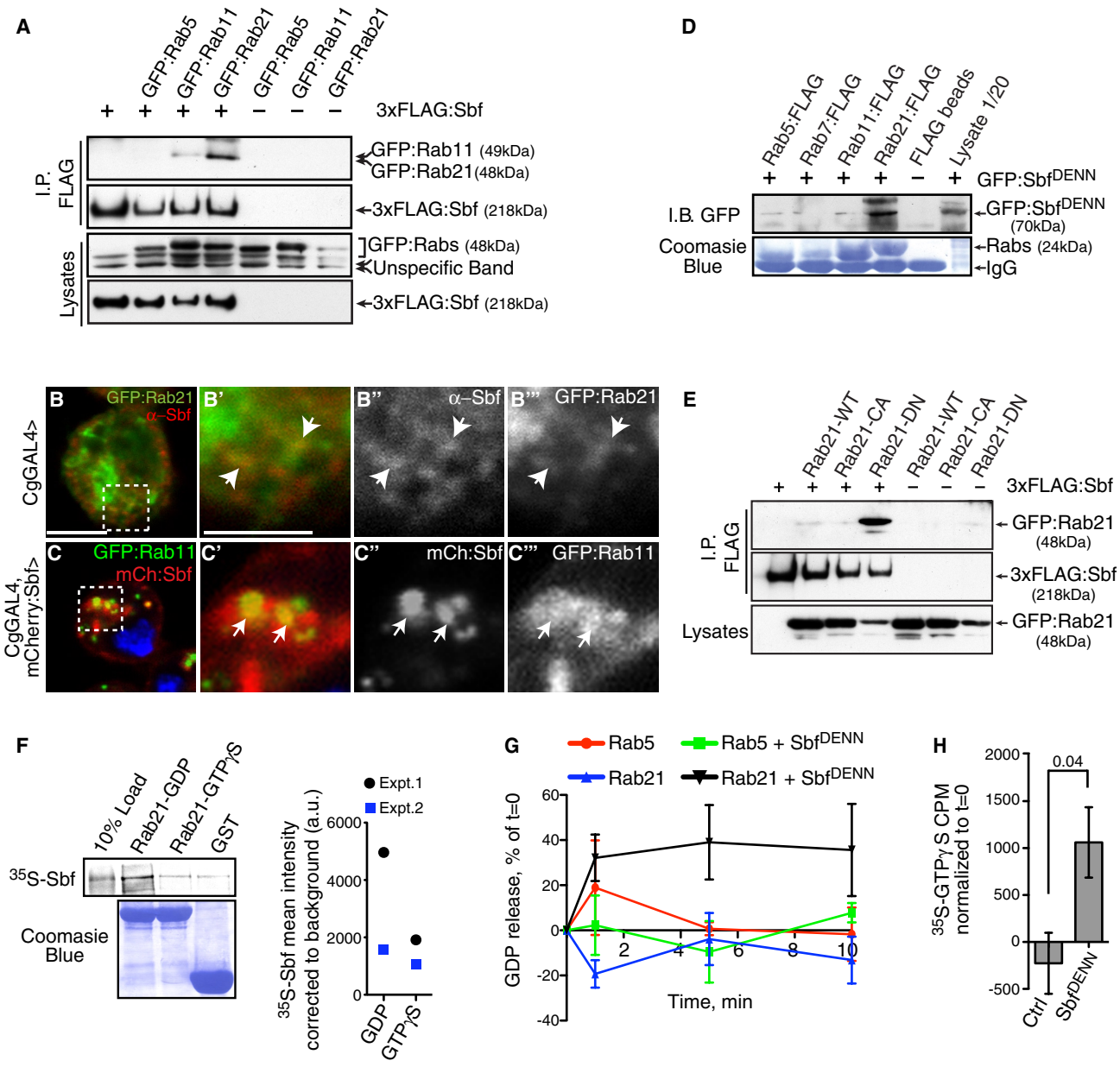

FIGURE 5: Sbf acts as a GEF for Rab21 activation and associates with Rab11-recycling endosomes. (A) Sbf interacts with Rab21,and weakly with Rab11. FLAG IP 3xFLAG:Sbf and immunoblot of coexpressed GFP-tagged Rab5, Rab11, and Rab21. (B–B‴) Endogenous Sbf colocalization with GFP:Rab21 and (C–C‴) mCherry:Sbf colocalization with GFP:Rab11 in macrophages. (D) Sbf DENN domain mediates interaction with Rab21. Rab:FLAG pull-downs of GFP:Sbf^{DENN} from Kc cell lysates, analyzed by anti-GFP immunoblot. Purified Rab proteins shown by Coomassie stain (bottom). (E, F) Sbf preferentially interacts with inactive Rab21. (E) FLAG IP 3xFLAG:Sbf and immunoblot of coexpressed GFP-tagged Rab21-WT, Rab21-CA, and Rab21-DN. (F) ^{35}S-labeled, in vitro–translated Sbf interacts with bacterially expressed Rab21 preloaded with GDP vs. with non-hydrolyzable GTPγS (top). Purified Rab21 protein shown by Coomassie stain (bottom). Plot of trends seen in two experiments. (G, H) Sbf has GEF activity for Rab21. (G) Sbf^{DENN} can release GDP from Rab21-GDP. GDP released over 10 min shown as percentage of total at t = 0 for Rab5 (red) or Rab21 (blue) alone or with Sbf^{DENN} (Rab5, green; Rab21; black); ±SEM, (H) Sbf^{DENN} can perform Rab21–GTP exchange. Counts per million (cpm) of ^{35}S-labeled Rab21-GTPγS after 1 min of incubation of GDP-Rab21 alone (Control) or together with Sbf-DENN protein, normalized to cpm at time 0; ±SEM. Bar, 5 μm, except 2.5 μm in crops.

endosomal membrane identities. In cultured cells, Sbf was able to coimmunoprecipitate Rab21 but not Rab5 (Figure 5A). A weaker physical interaction was also seen between Sbf and Rab11, an established component and regulator of recycling endosomes. In addition, Sbf colocalized to a similar extent with Rab21 and Rab5, which were found to be highly colocalized in mammalian cells (Simpson *et al.*, 2004), and to a greater extent with Rab11 (Figure 5, B and C), but not with other organelle markers (Supplemental Figure S4E). Taken together, these results suggest an Sbf involvement in endosomal trafficking.

Sbf is a Rab21 GEF

The Sbf and MTMR5/MTMR13 subfamily of pseudophosphatase proteins contain an N-terminal DENN domain (Figure 1A). DENN domains have been shown to exhibit Rab GEF activity (Allaire *et al.*, 2010; Yoshimura *et al.*, 2010). If Sbf is a GEF for an endosomal Rab, we predicted that an Sbf/Rab interaction would be preferential and direct for the GDP-Rab form and support GDP release with GTP exchange. First, we tested the ability of the Sbf^{DENN} domain to interact with any of the endosomal Rabs (Rab5, Rab7, Rab11, and Rab21). Of these four Rabs tested, only bacterially purified Rab21:FLAG was able to pull down Sbf^{DENN} from cell lysates (Figure 5D), indicating a specific Rab21–Sbf interaction mediated by the DENN domain. In agreement with the possibility of Sbf as a Rab21 GEF, we found a strong interaction by coIP between Sbf and a constitutively inactive form, Rab21–DN (dominant negative; Figure 5E). The Sbf interaction with Rab21-DN was much stronger than that seen with Rab21-WT, whereas we did not detect any interaction with a constitutively GTP-bound form, Rab21-CA (constitutive active). Conversely, we observed coIP of Sbf with both Rab11-WT and Rab11-CA and only weakly with Rab11-DN (Supplemental Figure S4F), further confirming an Sbf/Rab11 interaction independent of the Sbf DENN domain (Figure 5, A and D).

To address whether direct binding can occur between Sbf and Rab21, we assayed association between full-length, in vitro–translated Sbf with different nucleotide-loaded forms of recombinant Rab21. Radiolabeled Sbf showed a preferential interaction again—indicative here of direct binding—with purified GDP-loaded Rab21 but did not interact with nonhydrolyzable GTPγS-loaded Rab21 (Figure 5F). Finally, to address whether Sbf has Rab21 GEF activity, we monitored the ability for Sbf^{DENN} to promote Rab21 GDP release and GTP exchange in vitro. Sbf^{DENN} was sufficient to catalyze GDP-^{3}H release from preloaded Rab21 but not from Rab5 (Figure 5G) and to transfer GTPγS to GDP-loaded Rab21 (Figure 5H). In contrast, GDP-Rab21 protein incubated alone was deficient in GDP release and GTP transfer activity (Figure 5, G and H). The preferential, direct, and stimulatory interaction between Sbf and inactive Rab21 (and exclusion of an interaction with Rab21-GTP) demonstrates that Sbf pseudophosphatase is a Rab21 GEF in addition to having a direct regulatory role required for Mtm phosphatase function.

Sbf coregulates Rab21 and PI(3)P required for macrophage cortical dynamics

We next asked whether the discovered Rab21 interactions also reflect a shared functional role in macrophage protrusion formation. We found that, similar to *Sbf* or *mtm*, expression of *Rab21-WT* was sufficient to induce excess F-actin–based cell protrusions (Figure 6, A–C). The inability of Rab21-CA to induce a similar phenotype may be due to an inability to bind Sbf (Figure 5E) or to properly localize or cycle. Conversely, macrophage-specific expression of *Rab21-DN* or knockdown of *Rab21* by RNAi revealed a requirement for normal cell protrusion formation (Figure 6, C–E). The level of endogenous Rab21 protein depletion correlated with severity in the percentage of cells lacking protrusions (Supplemental Figure S5, A and B) and was further enhanced in combination with *Sbf* knockdown (Figure 6F). This shows that *Rab21*, like *Sbf* and *mtm*, is both necessary and sufficient for cell protrusion formation in macrophage remodeling.

To determine whether *Rab21* is important for the *Sbf* and *mtm* roles in this process, we performed epistasis analysis of the induced cell protrusions. Both *Sbf*- and *mtm*-induced formation of excess cell protrusions required *Rab21* function, as seen by the inhibition with either *Rab21-DN* or *Rab21* depletion (Figure 6, G–K, and Supplemental Figure S5, C and D). Similarly, *Rab21*-induced formation of excess protrusions required both *Sbf* and *mtm* functions (Figure 6, L–N, and Supplemental Figure S5, E and F). In all cases, disruption of the endogenous functions not only reverted the induced excess protrusions but also compromised the formation of normal protrusions, showing that either enforced PI(3)P turnover or Rab21 activity alone is not sufficient to compensate for loss of the other.

We further addressed the sufficiency of Sbf roles in either Rab21 or Mtm regulation to mediate induction of excess cell protrusions. The expression of truncated Sbf constructs deleted for either the N-terminus DENN domains or the C-terminus coiled-coil and PH domains could no longer induce excess protrusions (Figure 6O), indicating that the full-length Sbf interactions with both Rab21 and Mtm, respectively, are corequired. Taken together, these results demonstrate that Sbf acts via protein interactions with both Rab21 and Mtm and that all three genes are codependent in promoting cell protrusion formation. Of importance, this establishes a functionally significant regulatory relationship for a DENN domain–containing MTM pseudophosphatase toward a specific Rab.

Rab21 associates with PI(3)P endosomes and interacts with Mtm and Pi3K68D

To address a Rab21 relationship to the Sbf complex, we first investigated the Rab21 relationship to PI(3)P. Using the 2xFYVE biosensor, we found that Rab21, like Rab5, colocalized with PI(3)P but also to non–PI(3)P-containing membranes (Figure 7, A–D). Of interest, the expression of Rab21 or Rab5 altered the morphology of PI(3)P-containing membranes from rings to more collapsed and reticulated structures (Figure 7, A and B). In contrast, constitutively active forms did not (Figure 7, E and F), and moreover, only Rab5-CA led to swollen endosomes. The effects of *Rab21* or *Rab5* knockdown on PI(3)P-containing membranes were also distinct, exhibiting the known *Rab5* function in Vps34-synthesized endosomal PI(3)P versus an apparent *Rab21* effect on PI(3)P-membrane ring size and distribution (Figure 7, G and H)

We next investigated a Rab21 relationship to the Sbf complex through possible interactions with Pi3K68D or Mtm. Similar to Sbf, we detected coIP of the Rab21-DN or Rab21-WT forms with Mtm but only with Sbf coexpression (Supplemental Figure S5G). This suggests that Mtm and Rab21 interact indirectly through Sbf and that Sbf can exist in a co-complex with both Mtm and Rab21. Similarly, we detected coIP of Pi3K68D preferentially with the Rab21-DN form, even in the absence of Sbf coexpression (Figure 7, I–K). In contrast, Pi3K68D showed weak to no interaction with Rab5-DN, indicating a preferential association between class II PI3K and Rab21 (Figure 7, I and K). Thus Sbf, Pi3K68D, and Mtm each preferentially interacts with inactive Rab21 as well as influences regulation of a PI(3)P pool, further indicating coordination between PI(3)P and Rab21 regulation with shared consequences for cortical functions.

Endocytic recycling and Rac GTPase are important for Sbf complex role in protrusion formation

The complex of protein interactions and PI(3)P-related phenotypes point to an important Sbf role in endosomal membrane dynamics, suggesting that Sbf may promote membrane trafficking involved in endocytic recycling. This idea therefore also predicts a requirement for additional steps in endocytosis for normal cell protrusion formation. We found that inhibition of *shibire*, the single *Drosophila* dynamin GTPase involved in membrane scission, also led to lack of cell protrusions, implicating a requirement for internalization at the plasma membrane (Figure 8, A–C). Rab5 GTPase has widely established roles at early endosomes in the regulation of Vps34 kinase

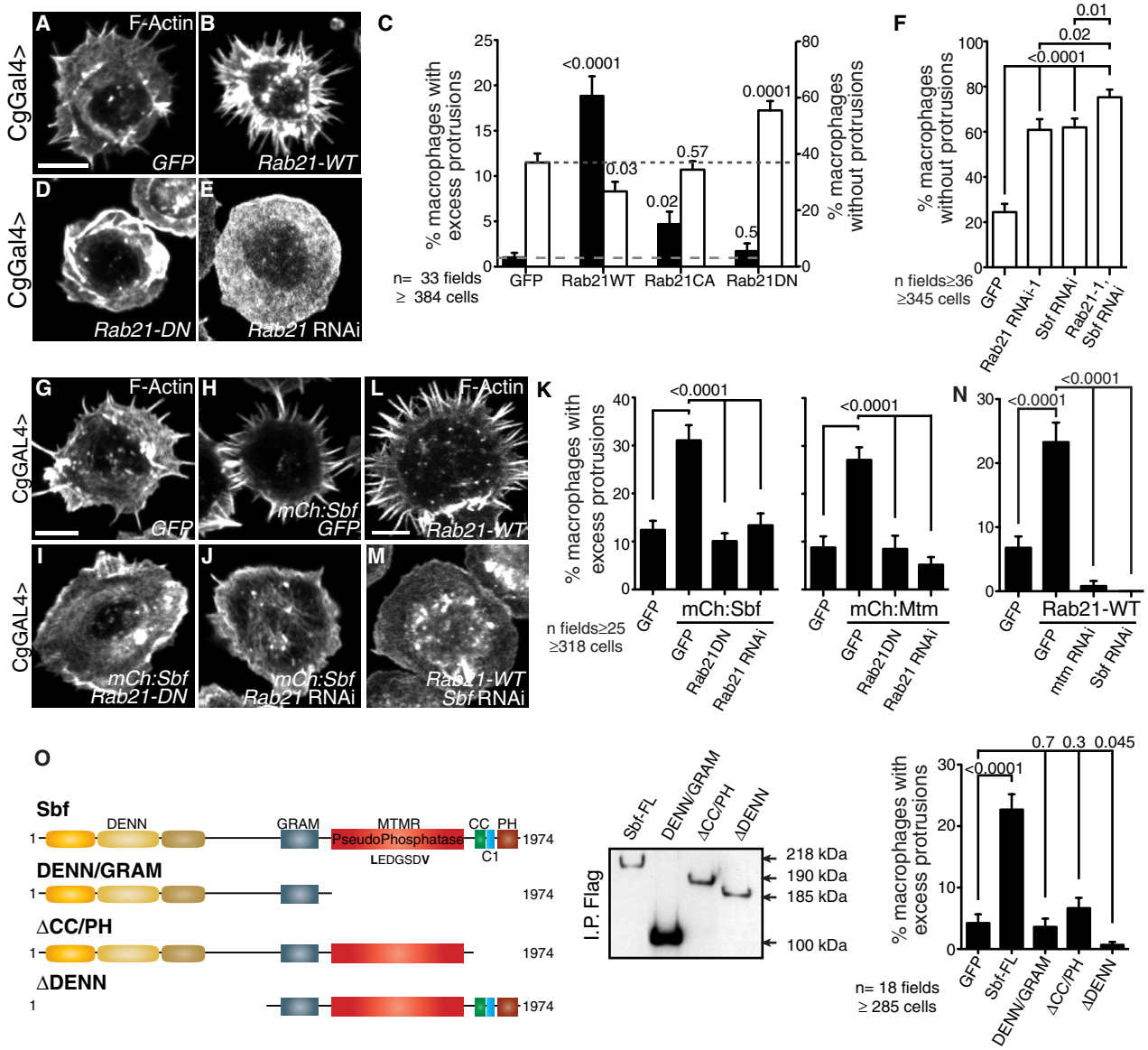

FIGURE 6: Rab21 GTPase activity functions with Sbf and Mtm to promote cell protrusions. (A, B, D, E, G–J, L, M) F-actin in primary macrophages. (A, G) Normal protrusions in control cells. (B) Excess protrusions with *Rab21-WT*. (C) Percentage of macrophages with excess (black) or lack (white) of protrusions upon expression of different *Rab21* forms; +SEM. Lack of protrusions with (D) *Rab21-DN* or (E) *Rab21* RNAi. (F) Percentage of macrophages without protrusions with *Rab21*, *Sbf* coRNAi; +SEM. (H) Excess protrusions induced by *Sbf*, suppressed by (I) *Rab21-DN* or (J) *Rab21* RNAi. (K) Percentage of macrophages with excess protrusions induced by *Sbf* (left) or *mtm* (right) and suppressed by coexpression of *Rab21-DN* or *Rab21* hairpin; +SEM; Cg-GAL4. (L) *Rab21-WT*–induced excess protrusions (M) suppressed by *Sbf* depletion. (N) Percentage of macrophages with excess protrusions. (O) FLAG-tagged Sbf full-length and truncated proteins. Immunoblot in Kc_{167} cells. Percentage of macrophages with excess cell protrusions; +SEM. Bars, 5 μm.

function and corecruitment of PI(3)P effectors (Christoforidis *et al.*, 1999). Unlike *Rab21*, we found that *Rab5* knockdown, as indicated by severe depletion of endosomal PI(3)P and dramatic increase in macrophage cell number (Figure 7G and Supplemental Figure S5, H and I), did not overtly affect cell protrusion formation (Figure 8, C and D). This suggests that *Rab21* can function independent of *Rab5* and may act on distinct endosomal compartments or microdomains or that low levels of Rab5 protein are sufficient for this role. Late steps in endocytosis represented by *Rab7* function also were not required in primary macrophages (Figure 8E), suggesting that an imbalance in degradation pathways likely is not central to the cortical phenotypes.

One trafficking route upon endosomal exit is through recycling endosomes marked by Rab11 GTPase, which broadly controls endocytic recycling back to the plasma membrane. Consistent with the identified Sbf–Rab11 protein interaction and colocalization (Figure 5, A–C, and Supplemental Figure S4, E and F), we found a requirement for *Rab11* in cell protrusion formation (Figure 8, C and F) and for *mtm*-induced formation of excess cell protrusions (Figure 8, G and H).

The specific Sbf-related cortical defects are typical of those described from perturbations of Rho GTPases that are central regulators of F-actin organization and cell protrusions. Accordingly, we found that expression of activated *Rac-CA* or *Rho-CA* was sufficient

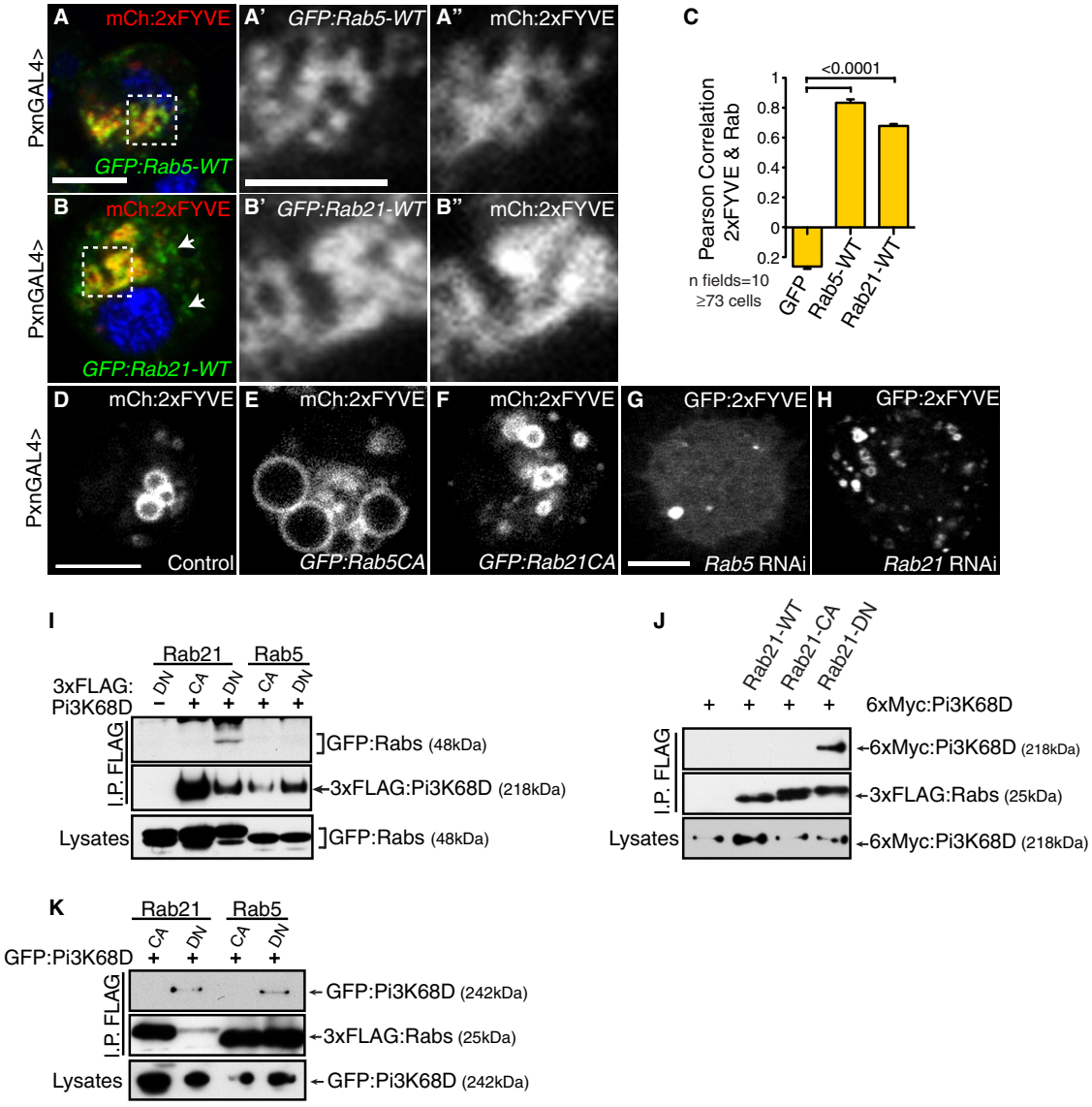

FIGURE 7: Rab21 affects PI(3)P endosomes and shares specific interaction with Pi3K68D. (A–C) Early endosomal Rabs colocalize with PI(3)P detected by mCherry:2xFYVE in primary macrophages. Colocalization of PI(3)P and (A) GFP:Rab5 and (B) GFP:Rab21. (C) Colocalization quantified as Pearson's r between mCherry:2xFYVE and GFP:Rab5 or GFP:Rab21; +SEM. (D) Normal PI(3)P distribution. (E–H) PI(3)P detected in cells with (E) Rab5-CA or (F) Rab21-CA expression and (G) *Rab5* or (H) *Rab21* RNAi. (I) IP 3xFLAG:Pi3K68D and immunoblot for GFP-tagged Rab21 or Rab5 forms (DN, CA). (J) IP 3xFLAG:Rab21 (WT, CA or DN) and immunoblot for 6xMyc:Pi3K68D. (K) IP 3xFLAG:Rab5 or Rab21 forms (CA,DN) and immunoblot for GFP:Pi3K68D. Bars, 5 μm, except 2.5 μm in crops.

to induce excess protrusions (Figure 8, I–L), similar to Sbf-complex gain-of-function conditions (Figures 1, 3, and 6). To address a role for specific Rho GTPases in Sbf-complex cortical functions, we performed epistasis studies. Expression of *Rac-CA*, but not *Rho-CA*, was able to rescue the loss of cell protrusions with *Sbf* knockdown (Figure 8, M–P). This suggests that Rac, either as a functionally important cargo or effector (Palamidessi *et al.*, 2008), is under endosomal regulation of the Sbf complex for normal GTPase activity

Sbf complex controls endosomal membrane cargo exit

We next asked whether turnover of specific cargo at the plasma membrane is affected by Sbf function. Transmembrane integrin receptor adhesion complexes are important for mammalian and fly macrophage spreading. Of interest, Rab21 was shown to regulate both integrin endocytic uptake and turnover in mammalian cells (Pellinen *et al.*, 2006, 2008; Mai *et al.*, 2011), and we showed that *mtm* and *Pi3K68D* coregulate integrin localization with turnover in fly and human muscle (Ribeiro *et al.*, 2011). To address a role for the *Sbf* pathway in integrin turnover in fly macrophages, we assayed endocytic uptake and trafficking of surface-labeled βPS-integrin using a specific antibody in a two-step staining method (Supplemental Figure S5, J and K). After 5- to 10-min pulses in uptake of surface-labeled βPS-integrin, no significant differences in internalized βPS-integrin were seen with *Sbf* and *mtm* depletion as compared with control cells (Figure 9, A and B). However, after a 30-min pulse in uptake, an accumulation of internalized βPS-integrin was nearly tripled with *Sbf* and *mtm* depletion versus in control cells (Figure 9, B–D), pointing to an *Sbf* role in promoting postendosomal trafficking. In contrast, *Rab21* RNAi led to a block in integrin endocytic uptake (Figure 9, B and E), consistent with reports in mammalian cells

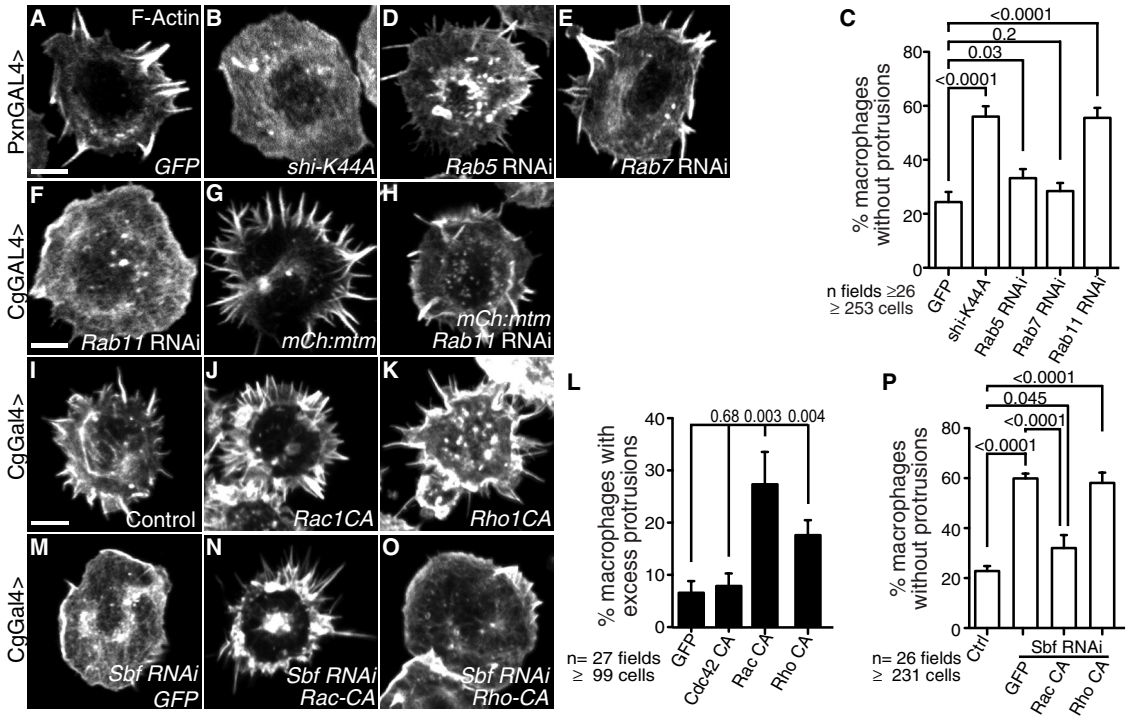

FIGURE 8: Sbf functions with a dynamin- and Rab11-mediated endocytic pathway important for cell protrusions. (A, B, D–K, M–O) F-Actin in primary macrophages. (A, I) Control. (B) Dominant-negative dynamin, *shi-K44A*. (C) Percentage of macrophages without cell protrusions; +SEM; Pxn-GAL4. (D) *Rab5* RNAi. (E) *Rab7* RNAi. (F) *Rab11* RNAi. (G) Excess protrusions with *mtm* expression, (H) suppressed by *Rab11* depletion. (J) *Rac-CA*. (K) *Rho-CA*. (L) Percentage of macrophages with excess cell protrusions; +SEM. (M) Lack of protrusions with *Sbf* RNAi, (N) suppressed by coexpressed *Rac-CA*, (O) but not *Rho-CA*. (P) Percentage of cells with lack of protrusions; +SEM. Bars, 5 µm.

(Pellinen *et al.*, 2006; Mai *et al.*, 2011), and confounding interpretations of Rab21 function at a later step. The distinct phenotypes seen here and the known integrin independence for cell protrusion formation (Kadandale *et al.*, 2010) suggest that *Sbf/mtm* and *Rab21* roles in integrin trafficking do not entirely account for Sbf complex–related roles in cell protrusion formation and that Rab21 may function at distinct Sbf-independent and Sbf-dependent endocytic steps.

Specific cortical functions for Sbf-coordinated PI(3)P and Rab21 endosomal regulation

We have shown that endocytic internalization and Rab21/Rab11-mediated endosomal trafficking is important for controlling the balance in the number of macrophage cell protrusions. In this pathway, the Sbf pseudophosphatase provides the mechanism for coordination between PI(3)P and Rab21 regulatory machinery involved in endocytic membrane dynamics and trafficking (Figure 10).

DISCUSSION

Using macrophage cell protrusions as a relevant in vivo model to study membrane regulation, we uncovered an endocytic trafficking mechanism controlled by an MTM pseudophosphatase. Our data show that the Sbf pseudophosphatase directly scaffolds Rab21 and Mtm, coordinating GTPase activation and PI(3)P dephosphorylation responsible for specification of an endocytic step with key cell regulatory roles (Figure 10).

In the simplest model, we envision that class II PI3-kinase either at the cell cortex or on distinct early endosomal vesicles or microdomains synthesizes a PI(3)P subpool that is the eventual target of Sbf–Mtm function. We speculate that the class II PI3-kinase may be distinguished from class III Vps34 endosomal function by being localized or stimulated for PI(3)P synthesis, for example, in conjunction with particular cargo selection or Sbf-complex interactions. This PI(3)P pool could serve to recruit effectors involved in protein sorting, such as specific sorting nexins, motor proteins, or endosome maturation. From our data, we favor a model in which subsequently Sbf promotes membrane traffic exiting from early to Rab11

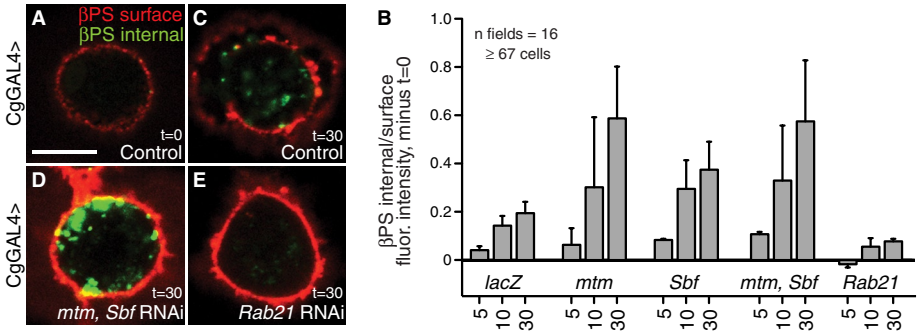

FIGURE 9: Sbf/Mtm promote endosomal membrane exit for cargo trafficking. (A, C–E) βPS-integrin uptake and trafficking assay, indicating βPS at surface (red) and cell interior (green). (A, C) Control cells at t = 0 and 30 min. (B) Fluorescence intensity ratio, βPS at cell surface:central with subtracted t = 0; +SEM. (D, E) Integrin uptake at t = 30 min in (D) *mtm*, *Sbf* coRNAi and (E) *Rab21* RNAi cells. Bars, 5 µm.

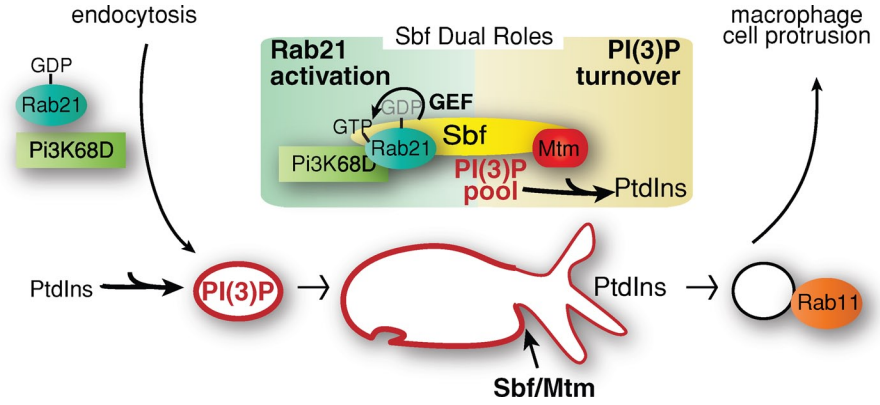

FIGURE 10: Model for Sbf coregulation of PI(3)P and Rab21 activation involved in endocytic trafficking. Class II PI3-kinase activity is required for normal PI(3)P levels and Sbf–Mtm functions (but not localization) in cell protrusion formation, and Pi3K68D/PI3KC2 protein associates with Sbf/MTMR13 and Rab21-GDP. Sbf directly acts as a GEF in the activation of Rab21, which localizes to PI(3)P endosomes. Sbf also affects Pi3K68D protein and directly recruits Mtm phosphatase activity required for PI(3)P turnover. Rab21 activity and PI(3)P turnover drive endosomal membrane exit. A shared Sbf requirement for and association with Rab11 suggests progression of exited membrane to Rab11-recycling endosomes.

endosomes. Sbf function for cell protrusions is likely required on endosomes, where Sbf simultaneously recruits Mtm phosphatase and activates Rab21 GTPase. The localized turnover of PI(3)P in conjunction with recruitment of unknown Rab21 effectors could drive membrane exit and/or phosphoinositide conversion from PI(3)P-containing endosomes. Sbf is also present at sites along the plasma membrane, suggesting that Sbf may remain on membranes throughout an endocytic and redelivery cycle or serve additional functions.

Our data demonstrate the importance of an MTM pseudophosphatase for the membrane recruitment of a specific MTM catalytic phosphatase function. We identified a novel and conserved interaction between Sbf/MTMR13 and Pi3K68D/PI3KC2α that is associated with cell membranes. This physical interaction further supports the demonstrated Pi3K68D functional relationship to Sbf–Mtm and points to Sbf as a mechanism to efficiently bridge specific sequential kinase and phosphatase functions. A central role for a common scaffold that is shared between kinase–phosphatase pairs is emerging as an important theme in phosphoinositide regulation with broader significance in human disease (Duex *et al.*, 2006; Chow *et al.*, 2007; Zhang *et al.*, 2007b; Chagpar *et al.*, 2010; Taguchi-Atarashi *et al.*, 2010). Of importance, our work raises the potential significance of class II PI3-kinase inhibition in treatment strategies for human MTMR2- or MTMR13-associated CMT4B neuropathies.

We showed that Sbf is a Rab21 GEF. The shared loss- and gain-of-function phenotypes for Sbf and Rab21 are consistent with Sbf serving a positive role to promote Rab21 function. As a GEF, Sbf may recruit and/or amplify Rab21 activity at a specific endosomal compartment, as described for cascading roles of different Rab5 GEFs (Horiuchi *et al.*, 1997; Sato *et al.*, 2005; Lodhi *et al.*, 2007; Zhu *et al.*, 2007). Rab21 shares sequence homology, endosomal localization, and trafficking functions with Rab5-related GTPases (Simpson *et al.*, 2004; Pellinen *et al.*, 2006; Zhang *et al.*, 2006; Egami and Araki, 2008), and here we show that Rab21 also colocalizes with PI(3)P and interacts with PI(3)P regulators. The shared interactions and functions with Sbf, Mtm, and Pi3K68D point to a specific early endosomal role for Rab21 in macrophage protrusion formation. Previously, Rab21 was shown to mark dynamic membrane tubules induced by PI(3)P depletion with PI3K inhibitors (Egami and Araki, 2008). We observed that Rab21 function altered PI(3)P membrane morphology, suggesting that Rab21 may act in parallel with or as an effector of PI(3)P. Rab21 was previously shown to directly bind to and promote integrin turnover in cell migration (Pellinen *et al.*, 2006) and to be required for endosomal to plasma membrane cargo delivery (Hooper *et al.*, 2010; Tower-Gilchrist *et al.*, 2011), and we recently described a role for Pi3K68D-Mtm in integrin trafficking during muscle remodeling (Ribeiro *et al.*, 2011). Here we show that Sbf-Mtm functions are also important for integrin trafficking in macrophages. Taken together, these results point to a mechanism in which Sbf–Mtm dephosphorylation of PI(3)P is specifically coupled to Rab21 activation and possible roles in selection or sorting of cargo(es) and/or membrane tubulation in endocytic recycling.

DENN-domain proteins recently were shown to act as Rab GEFs with restricted specificity (Wada *et al.*, 1997; Allaire *et al.*, 2010; Yoshimura *et al.*, 2010). The DENN domains from MTMR5/MTMR13 were shown to exhibit GEF activity toward Rab28 and weakly Rab5 (Yoshimura *et al.*, 2010). We demonstrate that the *Drosophila* Sbf DENN domain specifically interacts with Rab21—and not Rab11, Rab5, or Rab7—to promote Rab21-GDP to GTP exchange. Given that there is no obvious homologue of mammalian Rab28 in flies, evolutionary divergence is one explanation for the different MTMR13 and Sbf GEF specificities. Our work may point to a broader specificity for the DENN domain in the Sbf/MTMR subfamily. In addition, Rab21 has been shown to be a target of the Varp GEF (Zhang *et al.*, 2006). Therefore it is possible that Sbf Rab21 GEF activity and shared functions represent a subset of Sbf GEF targets, and conversely, Rab21 regulators. This is in keeping with examples of both the Rab5 and yeast Ypt1 GTPases, which can each be regulated by multiple GEFs within different protein complexes (Barrowman *et al.*, 2010). Of interest, an Sbf–Rab11 interaction that is independent of the Sbf DENN domain raises the possibility of a cascade of Sbf–Rab GTPase interactions in the progression of endosomal traffic.

Sbf serves dual roles in both phosphoinositide and Rab regulation. The ability of Sbf to associate with Mtm and Rab21 permits a mechanism for the coordination of PI(3)P turnover and Rab21 activation. A few examples are known for coupling PI(3)P kinase–phosphatase regulators and Rab GTPases (Cao *et al.*, 2007, 2008), phosphoinositide pools with the regulation of Rab GEF recruitment and Rab activity (Mizuno-Yamasaki *et al.*, 2010) and coincidence detection of joint phosphoinositide and Rab effectors (Di Paolo and De Camilli, 2006). One other example of coordination of specific Rab and phosphoinositide regulators, as we demonstrate here, was shown for p85 interactions as a scaffold for p110 and Pten (Chagpar *et al.*, 2010) and as a Rab5 GAP (Chamberlain *et al.*, 2004). Of importance, MTMR13 mutations within either the DENN or myotubularin-related domains are similarly associated with Charcot–Marie–Tooth 4B2 (Azzedine *et al.*, 2003; Senderek *et al.*, 2003), signifying the likely importance of both Rab GEF– and Mtm phosphatase–related functions in humans as well.

We demonstrate here the identity and mechanisms of endosomal trafficking machinery essential for cortical remodeling and cell protrusion formation. What remains to be determined is the identity of the protein cargo or lipids that mediate the underlying

structural remodeling and cell protrusion formation. We envision that trafficking of either a transmembrane receptor or Rac GTPase (Palamidessi *et al.*, 2008) could localize or activate signaling that controls F-actin regulators at the cortex. An alternative possibility is that the Sbf complex may have a more direct role in the recruitment of F-actin regulators. The assembly of Sbf/MTMR13 protein complexes with different catalytic proteins raises the possibility for a network of interactions affecting Rab and phosphoinositide functions, with implications for the balance of membrane trafficking in both normal and disease states. The expansion of the MTM family in metazoans, including the emergence of MTM pseudophosphatases, points to their likely roles in the regulation of different phosphoinositide pools that meets the membrane-trafficking demands for dynamic cell regulation.

MATERIALS AND METHODS

Cell staining and microscopy

Macrophages were bled from four or five wandering third-instar larvae 4 d after egg laying into 100 µl of complete medium (for live cell imaging) or phosphate-buffered saline (PBS) and allowed to attach to a glass coverslip for 1 h at 25°C. For F-actin visualization and immunofluorescence, macrophages were fixed 15 min in 3.7% formaldehyde, 1× PBS, washed twice for 5 min in PBS with 0.1% Triton X-100, and blocked for 60 min in PBSTB (PBS with 0.05% Tween 20 and 3% bovine serum albumen [BSA]). Cells were stained overnight at 4°C with Alexa Fluor 647 phalloidin (1:100; Invitrogen, Carlsbad, CA), with or without primary antibodies of affinity-purified rabbit anti-Sbf (1:400). Cells were washed five times with PBST, incubated for 1 h with anti-rabbit Alexa Fluor 488 (1:1000; Invitrogen) in PBSTB, stained 5 min with 4′,6-diamidino-2-phenylindole (1:1000; Invitrogen), and washed five times with PBST. Digital imaging was performed on a point-scanning microscope controlled by a FluoView program (FV1000; Olympus, Tokyo, Japan) using a 60×/1.2 numerical aperture (NA) Plan Apo N objective with a 1.5× or 2× zoom. ImageJ (National Institutes of Health, Bethesda, MD) was used to export tagged image file formats and three-dimensional reconstruction. Photoshop (Adobe, San Jose, CA) was used to adjust the levels and curves and to crop and resize images. For live cell imaging, spilled macrophages were kept in complete SM media containing 1:1000 Hoechst 33342 to stain nuclei.

Time-lapse microscopy

Macrophages were imaged every 15 s (11 *z*-planes spaced by 0.5 µm acquired per time point) for 5 min using a 60× oil/1.42 NA Plan Apo N objective on a spinning-disk fluorescence microscope (Ultraview VoX; PerkinElmer, Waltham, MA). Images were exported using Volocity software (PerkinElmer), and exported files were cropped and thresholded in Photoshop. Images were exported in ImageJ, in which they were cropped and thresholded.

FRAP analysis

Macrophages spilled into complete media were imaged at 5× zoom on scanning confocal microscope (FV1000). Five frames were acquired before photobleaching. Photobleaching was performed on equally sized rectangular regions of interest (ROI) with 20 repetitive scans using a 488-nm laser at 100% power. Images of the entire cell in each channel were immediately acquired after photobleaching at a 2.4-s interval for 110 s. ROI mean intensities were measured using FluoView software. FRAP analysis to determine normalized fluorescence intensity was performed as described (Goodwin and Kenworthy, 2005).

Integrin trafficking assay

Macrophages were isolated as described and incubated for 30 min at room temperature (RT). Cells were washed 2× in ice-cold media and incubated on ice for 60 min in media containing 5 µg/ml βPS-integrin CG.6G11 antibody (Developmental Studies Hybridoma Bank, University of Iowa, Iowa City, IA). Cells were washed 3× in ice-cold media and 2× in RT media and incubated for 0, 5, 10, and 30 min at 25°C to permit βPS uptake and trafficking. Macrophages were then washed 2× in ice-cold PBS, fixed in 4% paraformaldehyde for 30 min at RT, and washed 2× in PBS. Noninternalized integrin was labeled for 1 h at RT with 1:200 goat anti-mouse Alexa Fluor 546. Excess antibody was washed away with 5× PBS with 0.025% Tween 20. Remaining βPS-integrin was blocked for 1 h at RT using excess unconjugated goat anti-mouse antibody in PBS (1:7.5; Jackson ImmunoResearch Laboratories, West Grove, PA). Cells were then washed 5× in PBS–Tween 20 and subsequently permeabilized and blocked for 30 min at RT in blocking buffer (PBS containing 30% goat serum and 0.3% Triton X-100). Internalized βPS was labeled with goat anti-mouse Alexa Fluor 488 for 1 h in blocking buffer. Cells were washed 6× in PBS–Tween20 and 2× in PBS. Images were acquired in PBS at four different *z*-positions on a Zeiss LSM700 microscope (Carl Zeiss, Jena, Germany) using a 63×/1.40 NA Plan Apochromat objective. Image analysis and fluorescence quantification were carried out using CellProfiler. Integrin uptake was plotted as the mean internalized βPS subtracted by t = 0 from at least two independent experiments.

Cell culture, transfections, and RNAi

Drosophila Kc_{167} and S2R+ cells were cultured in Schneider's *Drosophila* medium (Invitrogen) containing 10% fetal bovine serum and 1% penicillin/streptomycin (Sigma-Aldrich, St. Louis, MO) at 24°C. Cells were transfected by calcium phosphate transfection (Invitrogen) or by FuGENE HD (GE Healthcare, Piscataway, NJ). pUAST constructs were transfected along with a metallothionein-*GAL4* plasmid. Transfected cells were incubated with 0.75 mM $CuSO_4$ in complete media for 6–8 h before immunoprecipitation. Generation of double-stranded RNAs and RNAi in cells were performed as previously described (Kiger *et al.*, 2003). RNAi efficiency after 3 d was determined by reverse transcriptase-PCR or Western blot analysis, as described (Velichkova *et al.*, 2010).

Antibody generation

Sbf protein fragment (amino acids 1866–1973), Pi3K68D protein fragment (2–236 amino acids), and Rab21PC (amino acids 1–222) were expressed in *Escherichia coli BL21*. Glutathione *S*-transferase (GST) fusion proteins were purified on glutathione–Sepharose 4B beads (GE Healthcare). For Sbf and Rab21PC, the GST moiety was cleaved with Factor Xa (New England BioLabs, Ipswich, MA), and Factor Xa was removed with the Factor Xa removal resin (Qiagen, Valencia, CA). For PI3K68D, the GST:Pi3K68D fusion protein was eluted with 25 mM reduced glutathione, 50 mM Tris-HCl, pH 8.8, 100 mM NaCl, and 0.1 mM dithiothreitol (DTT). Purified peptides were injected into rabbits (Robert Sargeant Antibody Services, Ramona, CA). For affinity purification of the Sbf antibody, 2 ml of serum was purified on an Sbf amino-linked column (Pierce, Rockford, IL).

Immunoprecipitations and immunoblots

Immunoprecipitations were carried out as described for the phosphatase assay, with these modifications. A total of 2.25×10^6 Kc_{167} cells or 5×10^5 S2R+ cells was plated per well of a six-well plate. Cells were lysed in 300 µl of lysis buffer, and 200 µl was used per

immunoprecipitation. After the fourth wash, proteins were eluted from beads in 2× SDS–PAGE loading buffer and heated at 95°C for 5 min. Antibodies used were mouse anti-GFP (1:1000; Santa Cruz Biotechnology, Santa Cruz, CA), mouse anti–α-tubulin (1:5000; Sigma-Aldrich), mouse anti-FLAG (1:2500; Sigma-Aldrich), mouse anti–Myc 9E10 (1:5000; Sigma-Aldrich) or rabbit anti-hemagglutinin (HA; 1:2500; Abcam, Cambridge, MA), followed by anti-mouse or anti-rabbit horseradish peroxidase (1:10,000; Invitrogen). Some Western blot scans were processed to realign lanes in the final figures. When such manipulations were needed, all adjustments on levels and contrasts were performed before realigning the lanes, thus preserving intensity differences between bands exactly as the raw scan before alignments. For assessment of protein extracts from primary tissues, we dissected 15–20 fat bodies from third-instar larvae with spilled macrophages in PBS. Tissue was homogenized in 50 mM 4-(2-hydroxyethyl)-1-piperazineethanesulfonic acid, pH 7.4, 150 mM KCl, 6.5% glycerol, 0.5 mM DTT, 0.1% Triton X-100, and 1× protease inhibitors and incubated on ice for 20 min. Extracts were spun at 13,200 rpm for 10 min at 4°C. Mouse MTMR13/Pi3KC2α immunoprecipitations were done as previously described (Robinson *et al.*, 2008) using anti-Pi3KC2α (611046; BD Biosciences, San Diego, CA) and anti-MTMR13 (116-AP) antibodies (Robinson and Dixon, 2005).

Phosphatase activity assay

Kc_{167} cells transfected with 3xFLAG:mtm and additional appropriate constructs were processed for immunoprecipitation and malachite green assay (Echelon Biosciences, Salt Lake City, UT), as previously described (Velichkova *et al.*, 2010). Because the in vitro phosphate release assay is conducted in the absence of ATP, experiments with coIP of Pi3K68D are not confounded by kinase activity. Briefly, transfected cells were washed twice with ice-cold PBS, lysed in 500 µl of lysis buffer, and spun at 13,000 rpm for 10 min; the supernatant was collected for IP using anti-FLAG M2 agarose beads (Sigma-Aldrich) for 2 h at 4°C, washed thrice with lysis buffer, once with lysis buffer without NP40, and twice in reaction buffer and then split into four tubes (two used for PI(3)P; two used for $PI(3,5)P_2$). Reaction mix (reaction buffer plus 50 µM phosphoinositides) was added to each tube, incubated for 20 min at 25°C, and then stopped by addition of 7 µl of 0.05 mM Na_3VO_4 and heated at 95°C for 2 min. Free phosphate in solution was measured by plate reader. Beads were loaded onto a 4–12% SDS–polyacrylamide gel (Invitrogen) and then stained with Sypro Ruby red stain to estimate the amount of protein. No ATP was present in the reaction buffer, preventing any contribution from Pi3K68D activity when present to phosphate release.

Cell fractionation

Cell fractionations were carried out as in Stegman and Robbins (2007), with these modifications. A total of 10×10^6 Kc_{167} cells plated in 2× 100-mm dishes per condition was lysed in 400 µl of GNE buffer (50 mM glycerophosphate, 10 mM NaF, 1.5 mM EGTA, and pH 7.6 with HCl). HSS1 fractions (cytosol) and HSP1 fractions (membrane) were used for immunoprecipitations. HSS1 was supplemented with 25 mM Tris-HCl, 1 mM EDTA, 0.1 mM ethylene glycol tetraacetic acid , 5 mM $MgCl_2$, 150 mM NaCl, 10% glycerol, 1% NP-40, 1 mM DTT, and 1× protease inhibitor (Sigma-Aldrich) to normalize to HSP1, which was resuspended in full lysis buffer. Immunoprecipitations were carried out as described, except that 750 µl was used as starting material.

In vitro protein binding

Direct GTPase binding assays were performed as in Christoforidis and Zerial (2000) with modifications. Using a scaled-down protocol, we loaded 200 µl of GST:Rab21PC beads with either GDP or GTPγS. Sbf was in vitro translated and labeled with ^{35}S-methionine using TNT T7 Quick Coupled Transcription/Translation from Promega (Madison, WI) according to instructions. To avoid GDP/GTP contamination, we purified 100 µl of TNT reaction through G-25 Sephadex in exchange buffer (50 mM Tris, pH 7.4, 5 mM EDTA, 100 mM NaCl, and 0.5 mg/ml BSA) and collected 150-µl fractions. The ^{35}S-Sbf–containing fractions (as determined by scintillation counting) were pooled. We added 75 µl of purified ^{35}S-Sbf to 25 µl of GST, GST:Rab21-GDP, or GST:Rab21-GTPγS in 500-µl nucleotide stabilization buffer (NS) containing 100 µM of either GDP or GTPγS and incubated it on a rotating wheel for 4 h. Beads were washed 4× in NS buffer containing 10 µM of the proper nucleotide, and proteins were eluted in 2× SDS–PAGE sample buffer. Proteins were loaded on an SDS–PAGE gel, transferred on a polyvinylidene fluoride (PVDF) membrane, and exposed on a Typhoon PhosphorImager (GE Healthcare). For Rab pull-downs, 5 µg of bacterially purified Rab:FLAG (Rab5, Rab7, Rab11, Rab21) immobilized on FLAG-M2 affinity gel was incubated with Kc cell lysate (as described for IPs) expressing GFP:Sbf^{DENN} (amino acids 1–508). Lysates in 400 µl were adjusted to a final GDP concentration of 100 µM and added to Rab beads. Beads were incubated for 4 h at 4°C on a nutator. After incubation, beads were washed 4× in 1 ml of NS containing 100 µM GDP. Protein elution, SDS–PAGE, transfer to PVDF membrane, and immunoblotting were carried out as described.

GDP release assay

Bacterially purified Rab5:FLAG and Rab21:FLAG (2 µg) immobilized on FLAG-M2 affinity gel were used for GDP release assay. Rabs were incubated in GDP loading buffer (10 µM GDP, 5 µCi GDP-^{3}H [PerkinElmer], 5 mM EDTA, 100 mM NaCl, and 20 mM Tris-HCl, pH 7.5) at 30°C for 15 min. GDP-Rabs were stabilized by addition of 10 mM $MgCl_2$ and centrifuged at 13,000 rpm, and the supernatant was removed. GDP-Rab beads were resuspended in 200 µl of GEF buffer (0.5 mg/ml BSA, 5 µM GTPyS, 0.5 mM DTT, 5 mM $MgCl_2$, 100 mM NaCl, and 20 mM Tris-HCl, pH 7.5). Each GDP-loaded Rab was split into two tubes and brought to 130 µl with GEF buffer or with ~100 nM Sbf^{DENN} (amino acids 1–508) and incubated at room temperature. At indicated time points, 20 µl was removed from the bead suspension and added to 1 ml of ice-cold wash buffer. Beads were washed 3× in 1 ml of wash buffer and after the last wash transferred to 5 ml of scintillation liquid and quantified in a scintillation counter. Values were adjusted as percentage of GDP released compared with time 0.

GTP exchange assay

HEK293T cells (10×, 100 mm) were transfected by calcium phosphate precipitation (Jean *et al.*, 2010) for expression of tagged *Drosophila* genes, FLAG:Rab21, or FLAG:Sbf^{DENN} domain (amino acids 1–508). At 24 h posttransfection, cells were lysed in 400 µl of lysis buffer (as described for IPs) per plate, and supernatants were pooled and added to 100 µl of FLAG-M2 affinity gel (Sigma-Aldrich) and incubated 2 h at 4°C on a rotating wheel. FLAG beads were washed 3× with complete lysis buffer, 1× with lysis buffer lacking NP-40, 3× with high-salt TBS (20 mM Tris-HCl, pH 7.4, 500 mM NaCl, and 1 mM DTT), and 3× with TBS (20 mM Tris-HCl, pH 7, 100 mM NaCl, and 1 mM DTT). FLAG-tagged proteins were eluted 5× with 100 µl of elution buffer (TBS containing 250 µg/ml 3xFLAG peptide) and dialyzed to remove the 3× peptide. Protein concentrations were estimated by comparing Coomassie staining to known control on a 10% SDS–PAGE gel. Proteins were flash frozen prior to GEF assay. GTP exchange assays were carried out as described in Allaire *et al.*

(2010). Rab21 (estimated 10 μM) was GDP loaded by incubation in GTPase loading buffer (40 μM GDP, 20 mM Tris-HCl, pH 7.4, 100 mM NaCl, 5 mM EDTA) at 30°C for 10 min. GDP-loaded GTPase was stabilized by10 mM $MgCl_2$. Exchange reactions were done at room temperature in 130-μl total volume containing 3 μM Rab21-GDP, 0.5 mg/ml BSA, 5 μM GTPγS, 1.25 μCi of GTPγS [^{35}S], 1250Ci/mmol, and 0.5 mM DTT, with or without 50 nM Sbf-DENN. At the indicated time, 20 μl of the reaction was removed, added to 1 ml of ice-cold wash buffer (20 mM Tris-HCl, pH 7.4, 100 mM NaCl, 20 mM $MgCl_2$), filtered through a Protran Nitrocellulose filter (Whatman, GE Healthcare), washed with 5 ml of wash buffer, and counted in a liquid scintillation counter. Results were normalized by subtracting values from the respective time 0.

Generation of DNA constructs

Full-length *Drosophila Sbf* cDNA or deletion mutants (DENN/GRAM nucleotides 1–2953; ΔDENN nucleotides 1359–5922 and ΔCC-PH 1–5079) were PCR amplified, cloned into the pENTR/D-TOPO entry vector (Invitrogen), subcloned by an LR recombination reaction into Gateway destination vectors pTGW-1075 (upstream activating sequence [UAS]-*eGFP:Sbf*, UAS-*eGFP:SbfDENN/GRAM*, UAS-*eGFP:SbfΔDENN*, UAS-*eGFP:SbfΔCC-PH*), pUAST-*mCherry-ccdB* (UAS-*mCherry:Sbf*), pTFW-1115 (UAS-*3xFLAG:Sbf*), pTMW-1107 (UAS-*6xMyc:Sbf*), pTHW-1099 (UAS-*3xHA:Sbf*), and pDEST17 (T7promoter-Sbf). The 3xFLAG-, 6xMyc-, and 3xHA-tagged forms of *Pi3K68D* cDNA were created from pEntr1a-*Pi3K68D-WT*, as described for Sbf. GST:Sbf-PH and GST:Pi3K68D N-terminal were cloned into pGEX5X-3 using the restriction enzymes *Bam*H1 and *Not*I. Rab21 constructs were created by PCR amplification from Kc_{167} cDNA. The *Rab21-RC* transcript was amplified and cloned into pENTR/dTOPO gateway vector. GFP- and FLAG-tagged constructs were made as described for Sbf. *Rab21-Q73L* (constitutively active, referred to as *Rab21-CA*) or *Rab21-T27N* (dominant negative, referred to as *Rab21-DN*) constructs were created from the pENTR/dTOPO-*Rab21PC* vector with gene-specific mutagenic primers using the same method as for *PI3K68D-D1457A*. GST-Rab21PC was obtained by PCR amplification from the pENTR/dTOPO-*Rab21PC* with primers harboring the restriction enzyme sites. The PCR fragment was digested by *Bgl*II/*Not*I and ligated into pGEX5X-3 digested with *Bam*HI/*Not*I. All DNA constructs were validated by DNA sequencing and protein expression.

Drosophila strains

Genotypes used in this study include the following: 1) UAS-IRmtm$^{3.1}$/CyO, 2) w; UAS-mCherry:mtm^{7}, 3) w; UAS-eGFP:mtm^{4}, 4) w; UAS-mCherry:Pi3K68D$^{2.1}$/CyO, 5) w;UAS-Pi3K68D:eGFP/CyO, and 6) w; Cg-GAL4, UAS-mCherry:mtm^{7} (Velichkova *et al.*, 2010), 7) w; UAS-IRSbf^{22317} ("Sbf RNAi"), 8) w[1118]; UAS-IRPi3K68D^{16240}, 9) w; UAS-IRCG14411^{17576}, 10) w; UAS-IRCG5026^{34915}, 11) w; UAS-IRRab21^{32941} ("Rab21 RNAi-1"), 12) w; UAS-IRRab21^{109991} ("Rab21 RNAi-2"), 13) w;UAS-IRRab5^{103945}, 14) w;UAS-IRRab7^{40338}, and 15) w;UAS-IR-Rab11^{108382} (Dietzl *et al.*, 2007), 16) y^{1} sc* v^{1}; P{TRiP.HMS00414}attP2 (Bloomington 32419; "Sbf RNAi-2"), 17) y^{1} v^{1}; P{TRiP.JF03338}attP2 (Bloomington 29403; "Rab21 RNAi-3"), and 18) w[1118]; P{w[+mC] = Cg-GAL4.A}^{2} (Asha *et al.*, 2003), 19) w; Cg-GAL4, P{w[+mC] = UAS-2xEGFP}^{AH2}, 20) w; Pxn-GAL4$^{8.1.1}$, 21) w; Pxn-GAL4$^{8.1.1}$, UAS-GFP (Stramer *et al.*, 2005), 22) w[1118]; P{w[+mC] = UAS-lacZ.B}Bg4-1-2, 23) w; UAS-GFP:myc:2xFYVE/CyO, and 24) w; UAS-GFP:Rab5 (Wucherpfennig *et al.*, 2003), and 25) w; UAS-GFP:Rab7/CyO (Entchev *et al.*, 2000), 26) y[1]w[*] P{w[+mC] = UAS-shi.K44A}4-1; P{w[+mC] = UAS-shi.K44A}3-7 (Bloomington 5811), and 27) w; UAS-Cdc42.V12^{LL1} (Bloomington BL4854), and 28) w; dRac1V12.

New genotypes generated during this study include the following: 1) w; UAS-IRSbf^{V22317}, UAS-eGFP, 2) w; UAS-IRmtm$^{3.1}$, UAS-IRSbf^{22317}, 3) w; UAS-mCherry:Sbf^{5}, 4) w;UAS-eGFP:Sbf^{2}, 5) w; PxnGal4$^{8.1.1}$, UAS-mCherry:myc:2xFYVE^{2}, 6) w; PxnGal4$^{8.1.1}$, eGFP:myc:2xFYVE^{1}, 7) w; Cg-Gal4, UAS-mCherry:Sbf^{5}, 8) w; Pxn-GAL4$^{8.1.1}$, UAS-eGFP:Sbf^{2}, 9) w; Pxn-GAL4$^{8.1.1}$, UAS-Pi3K68D:eGFP, 10) w; UAS-IRSbf^{22317}; UAS-IRPi3K68D^{16240}, 11) w[1118];UAS-eGFP:mtm^{7}, UAS-mCherry:Sbf^{6}, 12) w[1118];UAS-IRSbf^{22317}, UAS-mCherrySbf^{5}, 13) w; Cg-Gal4; UAS-IRPi3K68D^{16240}, 14) w; UAS-GFP:Rab21-WT^{7}, 15) w; UAS-GFP:Rab21Q73L^{2} ("Rab21-CA"), 16) w; UAS-GFP:Rab21T27N^{4} ("Rab21-DN"), 17) w; Cg-Gal4, UAS-GFP:Rab21-WT^{7}, 18) w; UAS-3xFLAG:Sbf^{2}, 19) w; UAS-IRSbf^{22317}, IRRab21^{32941}/Cyo^{17}, 20) w; UAS-IRSbf^{22317}; UAS-Rac1V12, 21) w; CgGal4; Rho1V14/TM6C,Sb,Tb, 22) w; UAS-eGFP:Sbf-DENN/GRAM^{6}, 23) w; UAS-eGFP:SbfΔCC-PH^{1}, and 24) w; UAS-eGFPΔDENN^{4}.

Determination of animal viability

Crosses were performed at 29°C. Flies were incubated for 24 h to allow sufficient egg laying, parents were removed, and progeny were allowed to develop. The numbers of animals reaching pupal, pharate, and adult stages were counted for each genotype.

Larval macrophage counts and distribution

To determine macrophage counts, individual third-instar larvae were bled into 15 μl of PBS with trypan blue to stain dying cells, and a hemocytometer was used to determine total viable macrophages per larva. To image sessile hemocytes, we mounted wandering third-instar larvae dorsal side up on double-sided tape and affixed them under a glass coverslip, as described (Velichkova *et al.*, 2010).

Statistical methods

CellProfiler software (www.cellprofiler.org/) was used to determine the ratio of PI(3)P-membrane area to cytoplasmic area per cell. Briefly, cell edges were first identified to measure total cell area. A mask of thresholded GFP:2xFYVE signal was subtracted from the total cell area, giving the cytoplasmic area unoccupied by the GFP:2xFYVE signal (masked cytoplasmic area). In Excel (Microsoft, Redmond, WA), 1 – (masked cytoplasmic area/total cell area) was used to determine the ratio of GFP:2xFYVE/cytoplasmic area. This measurement accounts for both the number and size of the GFP:2xFYVE-identified membrane while also correcting for differences in cell size. In addition, GFP:2xFYVE rings were manually counted from the same experimental sets. Prism software (GraphPad Software, La Jolla, CA) was used to calculate the mean-normalized GFP:2xFYVE area from ≥108 cells across two independent experiments, SE, and Student's *t* test. Cell morphology of F-actin–labeled spread macrophages was assessed manually and categorized as normal, with excess, or with no protrusions. Cells with excess protrusions were identified as those exhibiting tightly spaced protrusions, with approximately >20 protrusions. Cells were scored from within entire image fields from three or more experiments, and results were plotted as the mean percentage of cells in each category. Prism was used to calculate SEM and Student's *t* test. Colocalization was quantified using Pearson's r with CellProfiler. For phosphatase assays, a Student's *t* test was used in Figure 2C and Supplemental S4C, and a one-sample *t* test was used in Figure 2B.

ACKNOWLEDGMENTS

We thank Marcos González-Gaitán, Michael Galko, Patrick Allaire, Peter McPherson, the *Drosophila* Genomics Resource Center, the Bloomington *Drosophila* Stock Center, and the Vienna *Drosophila* RNAi Center for reagents. We thank Joe Juan, Tran Nguyen, and

Ryan Roxas for technical assistance; Jeffrey Keil and Gentry Patrick for advice on membrane fractionation; Peter Novick for advice on Rab GTPase GEF assays; and Carl St-Pierre for help with FRAP analysis. We thank Rick Firtel, Peter Novick, Seth Field, and members of our laboratory for helpful comments on the manuscript. Imaging was conducted in part at the University of California, San Diego, Neuroscience Microscopy Shared Imaging Facility, which is supported by National Institutes of Health Grant P30 NS047101. This research was supported by a Fonds de la Recherche en Santé du Québec Award to S.J., a Packard Foundation Grant 2005-29096 to A.A.K., and National Institutes of Health Grant RO1 GM078176 to A.A.K.

REFERENCES

Allaire PD, Marat AL, Dall'Armi C, Di Paolo G, McPherson PS, Ritter B (2010). The Connecdenn DENN domain: a GEF for Rab35 mediating cargo-specific exit from early endosomes. Mol Cell 37, 370–382.

Asha H, Nagy I, Kovacs G, Stetson D, Ando I, Dearolf CR (2003). Analysis of Ras-induced overproliferation in *Drosophila* hemocytes. Genetics 163, 203–215.

Azzedine H *et al.* (2003). Mutations in MTMR13, a new pseudophosphatase homologue of MTMR2 and Sbf1, in two families with an autosomal recessive demyelinating form of Charcot-Marie-Tooth disease associated with early-onset glaucoma. Am J Hum Genet 72, 1141–1153.

Backer JM (2008). The regulation and function of class III PI3Ks: novel roles for Vps34. Biochem J 410, 1–17.

Barrowman J, Bhandari D, Reinisch K, Ferro-Novick S (2010). TRAPP complexes in membrane traffic: convergence through a common Rab. Nat Rev Mol Cell Biol 11, 759–763.

Behnia R, Munro S (2005). Organelle identity and the signposts for membrane traffic. Nature 438, 597–604.

Berger P, Berger I, Schaffitzel C, Tersar K, Volkmer B, Suter U (2006). Multilevel regulation of myotubularin-related protein-2 phosphatase activity by myotubularin-related protein-13/set-binding factor-2. Hum Mol Genet 15, 569–579.

Berger P, Bonneick S, Willi S, Wymann M, Suter U (2002). Loss of phosphatase activity in myotubularin-related protein 2 is associated with Charcot-Marie-Tooth disease type 4B1. Hum Mol Genet 11, 1569–1579.

Bolino A *et al.* (2000). Charcot-Marie-Tooth type 4B is caused by mutations in the gene encoding myotubularin-related protein-2. Nat Genet 25, 17–19.

Cao C, Backer JM, Laporte J, Bedrick EJ, Wandinger-Ness A (2008). Sequential actions of myotubularin lipid phosphatases regulate endosomal PI(3)P and growth factor receptor trafficking. Mol Biol Cell 19, 3334–3346.

Cao C, Laporte J, Backer JM, Wandinger-Ness A, Stein MP (2007). Myotubularin lipid phosphatase binds the hVPS15/hVPS34 lipid kinase complex on endosomes. Traffic 8, 1052–1067.

Chagpar RB, Links PH, Pastor MC, Furber LA, Hawrysh AD, Chamberlain MD, Anderson DH (2010). Direct positive regulation of PTEN by the p85 subunit of phosphatidylinositol 3-kinase. Proc Natl Acad Sci USA 107, 5471–5476.

Chamberlain MD, Berry TR, Pastor MC, Anderson DH (2004). The p85alpha subunit of phosphatidylinositol 3′-kinase binds to and stimulates the GTPase activity of Rab proteins. J Biol Chem 279, 48607–48614.

Chow CY *et al.* (2007). Mutation of FIG4 causes neurodegeneration in the pale tremor mouse and patients with CMT4J. Nature 448, 68–72.

Christoforidis S, Miaczynska M, Ashman K, Wilm M, Zhao L, Yip SC, Waterfield MD, Backer JM, Zerial M (1999). Phosphatidylinositol-3-OH kinases are Rab5 effectors. Nat Cell Biol 1, 249–252.

Christoforidis S, Zerial M (2000). Purification and identification of novel Rab effectors using affinity chromatography. Methods 20, 403–410.

Dang H, Li Z, Skolnik EY, Fares H (2004). Disease-related myotubularins function in endocytic traffic in *Caenorhabditis elegans*. Mol Biol Cell 15, 189–196.

Di Paolo G, De Camilli P (2006). Phosphoinositides in cell regulation and membrane dynamics. Nature 443, 651–657.

Dietzl G *et al.* (2007). A genome-wide transgenic RNAi library for conditional gene inactivation in *Drosophila*. Nature 448, 151–156.

Duex JE, Tang F, Weisman LS (2006). The Vac14p-Fig4p complex acts independently of Vac7p and couples PI3,5P2 synthesis and turnover. J Cell Biol 172, 693–704.

Egami Y, Araki N (2008). Characterization of Rab21-positive tubular endosomes induced by PI3K inhibitors. Exp Cell Res 314, 729–737.

Entchev EV, Schwabedissen A, Gonzalez-Gaitan M (2000). Gradient formation of the TGF-beta homolog Dpp. Cell 103, 981–991.

Falasca M, Hughes WE, Dominguez V, Sala G, Fostira F, Fang MQ, Cazzolli R, Shepherd PR, James DE, Maffucci T (2007). The role of phosphoinositide 3-kinase C2alpha in insulin signaling. J Biol Chem 282, 28226–28236.

Firestein R, Nagy PL, Daly M, Huie P, Conti M, Cleary ML (2002). Male infertility, impaired spermatogenesis, and azoospermia in mice deficient for the pseudophosphatase Sbf1. J Clin Invest 109, 1165–1172.

Gaidarov I, Smith ME, Domin J, Keen JH (2001). The class II phosphoinositide 3-kinase C2alpha is activated by clathrin and regulates clathrin-mediated membrane trafficking. Mol Cell 7, 443–449.

Gary JD, Wurmser AE, Bonangelino CJ, Weisman LS, Emr SD (1998). Fab1p is essential for PtdIns(3)P 5-kinase activity and the maintenance of vacuolar size and membrane homeostasis. J Cell Biol 143, 65–79.

Goodwin JS, Kenworthy AK (2005). Photobleaching approaches to investigate diffusional mobility and trafficking of Ras in living cells. Methods 37, 154–164.

Grant BD, Donaldson JG (2009). Pathways and mechanisms of endocytic recycling. Nat Rev Mol Cell Biol 10, 597–608.

Grosshans BL, Ortiz D, Novick P (2006). Rabs and their effectors: achieving specificity in membrane traffic. Proc Natl Acad Sci USA 103, 11821–11827.

Hooper S, Gaggioli C, Sahai E (2010). A chemical biology screen reveals a role for Rab21-mediated control of actomyosin contractility in fibroblast-driven cancer invasion. Br J Cancer 102, 392–402.

Horiuchi H *et al.* (1997). A novel Rab5 GDP/GTP exchange factor complexed to Rabaptin-5 links nucleotide exchange to effector recruitment and function. Cell 90, 1149–1159.

Jean S, Mikryukov A, Tremblay MG, Baril J, Guillou F, Bellenfant S, Moss T (2010). Extended-synaptotagmin-2 mediates FGF receptor endocytosis and ERK activation in vivo. Dev Cell 19, 426–439.

Kadandale P, Stender JD, Glass CK, Kiger AA (2010). Conserved role for autophagy in Rho1-mediated cortical remodeling and blood cell recruitment. Proc Natl Acad Sci USA 107, 10502–10507.

Kiger A, Baum B, Jones S, Jones M, Coulson A, Echeverri C, Perrimon N (2003). A functional genomic analysis of cell morphology using RNA interference. J Biol 2, 27.

Kim SA, Taylor GS, Torgersen KM, Dixon JE (2002). Myotubularin and MTMR2, phosphatidylinositol 3-phosphatases mutated in myotubular myopathy and type 4B Charcot-Marie-Tooth disease. J Biol Chem 277, 4526–4531.

Kim SA, Vacratsis PO, Firestein R, Cleary ML, Dixon JE (2003). Regulation of myotubularin-related (MTMR)2 phosphatidylinositol phosphatase by MTMR5, a catalytically inactive phosphatase. Proc Natl Acad Sci USA 100, 4492–4497.

Laporte J, Blondeau F, Buj-Bello A, Tentler D, Kretz C, Dahl N, Mandel JL (1998). Characterization of the myotubularin dual specificity phosphatase gene family from yeast to human. Hum Mol Genet 7, 1703–1712.

Laporte J, Hu LJ, Kretz C, Mandel JL, Kioschis P, Coy JF, Klauck SM, Poustka A, Dahl N (1996). A gene mutated in X-linked myotubular myopathy defines a new putative tyrosine phosphatase family conserved in yeast. Nat Genet 13, 175–182.

Lee HW, Kim Y, Han K, Kim H, Kim E (2010). The phosphoinositide 3-phosphatase MTMR2 interacts with PSD-95 and maintains excitatory synapses by modulating endosomal traffic. J Neurosci 30, 5508–5518.

Lindmo K, Stenmark H (2006). Regulation of membrane traffic by phosphoinositide 3-kinases. J Cell Sci 119, 605–614.

Lodhi IJ, Chiang SH, Chang L, Vollenweider D, Watson RT, Inoue M, Pessin JE, Saltiel AR (2007). Gapex-5, a Rab31 guanine nucleotide exchange factor that regulates Glut4 trafficking in adipocytes. Cell Metab 5, 59–72.

Lorenzo O, Urbe S, Clague MJ (2006). Systematic analysis of myotubularins: heteromeric interactions, subcellular localisation and endosome-related functions. J Cell Sci 119, 2953–2959.

MacDougall LK, Domin J, Waterfield MD (1995). A family of phosphoinositide 3-kinases in *Drosophila* identifies a new mediator of signal transduction. Curr Biol 5, 1404–1415.

Maffucci T, Cooke FT, Foster FM, Traer CJ, Fry MJ, Falasca M (2005). Class II phosphoinositide 3-kinase defines a novel signaling pathway in cell migration. J Cell Biol 169, 789–799.

Mai A, Veltel S, Pellinen T, Padzik A, Coffey E, Marjomaki V, Ivaska J (2011). Competitive binding of Rab21 and p120RasGAP to integrins regulates receptor traffic and migration. J Cell Biol 194, 291–306.

Mizuno-Yamasaki E, Medkova M, Coleman J, Novick P (2010). Phosphatidylinositol 4-phosphate controls both membrane recruitment and a regulatory switch of the Rab GEF Sec2p. Dev Cell 18, 828–840.
Palamidessi A, Frittoli E, Garre M, Faretta M, Mione M, Testa I, Diaspro A, Lanzetti L, Scita G, Di Fiore PP (2008). Endocytic trafficking of Rac is required for the spatial restriction of signaling in cell migration. Cell 134, 135–147.
Pellinen T, Arjonen A, Vuoriluoto K, Kallio K, Fransen JA, Ivaska J (2006). Small GTPase Rab21 regulates cell adhesion and controls endosomal traffic of beta1-integrins. J Cell Biol 173, 767–780.
Pellinen T, Ivaska J (2006). Integrin traffic. J Cell Sci 119, 3723–3731.
Pellinen T *et al.* (2008). Integrin trafficking regulated by Rab21 is necessary for cytokinesis. Dev Cell 15, 371–385.
Ribeiro I, Yuan L, Tanentzapf G, Dowling JJ, Kiger A (2011). Phosphoinositide regulation of integrin trafficking required for muscle attachment and maintenance. PLoS Genet 7, e1001295.
Robinson FL, Dixon JE (2005). The phosphoinositide-3-phosphatase MTMR2 associates with MTMR13, a membrane-associated pseudophosphatase also mutated in type 4B Charcot-Marie-Tooth disease. J Biol Chem 280, 31699–31707.
Robinson FL, Dixon JE (2006). Myotubularin phosphatases: policing 3-phosphoinositides. Trends Cell Biol 16, 403–412.
Robinson FL, Niesman IR, Beiswenger KK, Dixon JE (2008). Loss of the inactive myotubularin-related phosphatase Mtmr13 leads to a Charcot-Marie-Tooth 4B2-like peripheral neuropathy in mice. Proc Natl Acad Sci USA 105, 4916–4921.
Sato M, Sato K, Fonarev P, Huang CJ, Liou W, Grant BD (2005). *Caenorhabditis elegans* RME-6 is a novel regulator of RAB-5 at the clathrin-coated pit. Nat Cell Biol 7, 559–569.
Senderek J, Bergmann C, Weber S, Ketelsen UP, Schorle H, Rudnik-Schoneborn S, Buttner R, Buchheim E, Zerres K (2003). Mutation of the SBF2 gene, encoding a novel member of the myotubularin family, in Charcot-Marie-Tooth neuropathy type 4B2/11p15. Hum Mol Genet 12, 349–356.
Silhankova M, Port F, Harterink M, Basler K, Korswagen HC (2010). Wnt signalling requires MTM-6 and MTM-9 myotubularin lipid-phosphatase function in Wnt-producing cells. EMBO J 29, 4094–4105.
Simpson JC, Griffiths G, Wessling-Resnick M, Fransen JA, Bennett H, Jones AT (2004). A role for the small GTPase Rab21 in the early endocytic pathway. J Cell Sci 117, 6297–6311.
Srivastava S *et al.* (2009). The class II phosphatidylinositol 3 kinase C2beta is required for the activation of the K+ channel KCa3.1 and CD4 T-cells. Mol Biol Cell 20, 3783–3791.
Stegman M, Robbins D (2007). Biochemical fractionation of *Drosophila* cells. Methods Mol Biol 397, 203–213.
Stramer B, Wood W, Galko MJ, Redd MJ, Jacinto A, Parkhurst SM, Martin P (2005). Live imaging of wound inflammation in *Drosophila* embryos reveals key roles for small GTPases during in vivo cell migration. J Cell Biol 168, 567–573.
Taguchi-Atarashi N, Hamasaki M, Matsunaga K, Omori H, Ktistakis NT, Yoshimori T, Noda T (2010). Modulation of local PtdIns3P levels by the PI phosphatase MTMR3 regulates constitutive autophagy. Traffic 11, 468–478.
Taylor GS, Maehama T, Dixon JE (2000). Inaugural article: myotubularin, a protein tyrosine phosphatase mutated in myotubular myopathy, dephosphorylates the lipid second messenger, phosphatidylinositol 3-phosphate. Proc Natl Acad Sci USA 97, 8910–8915.
Tersar K, Boentert M, Berger P, Bonneick S, Wessig C, Toyka KV, Young P, Suter U (2007). Mtmr13/Sbf2-deficient mice: an animal model for CMT4B2. Hum Mol Genet 16, 2991–3001.
Tower-Gilchrist C, Lee E, Sztul E (2011). Endosomal trafficking of the G protein-coupled receptor somatostatin receptor 3. Biochem Biophys Res Commun. 413, 555–560.
Tsujita K, Itoh T, Ijuin T, Yamamoto A, Shisheva A, Laporte J, Takenawa T (2004). Myotubularin regulates the function of the late endosome through the gram domain-phosphatidylinositol 3,5-bisphosphate interaction. J Biol Chem 279, 13817–13824.
Velichkova M, Juan J, Kadandale P, Jean S, Ribeiro I, Raman V, Stefan C, Kiger AA (2010). *Drosophila* Mtm and class II PI3K coregulate a PI(3)P pool with cortical and endolysosomal functions. J Cell Biol 190, 407–425.
Wada M, Nakanishi H, Satoh A, Hirano H, Obaishi H, Matsuura Y, Takai Y (1997). Isolation and characterization of a GDP/GTP exchange protein specific for the Rab3 subfamily small G proteins. J Biol Chem 272, 3875–3878.
Wheeler M, Domin J (2001). Recruitment of the class II phosphoinositide 3-kinase C2beta to the epidermal growth factor receptor: role of Grb2. Mol Cell Biol 21, 6660–6667.
Wucherpfennig T, Wilsch-Brauninger M, Gonzalez-Gaitan M (2003). Role of *Drosophila* Rab5 during endosomal trafficking at the synapse and evoked neurotransmitter release. J Cell Biol 161, 609–624.
Yoshimura S, Gerondopoulos A, Linford A, Rigden DJ, Barr FA (2010). Family-wide characterization of the DENN domain Rab GDP-GTP exchange factors. J Cell Biol 191, 367–381.
Zhang J, Schulze KL, Hiesinger PR, Suyama K, Wang S, Fish M, Acar M, Hoskins RA, Bellen HJ, Scott MP (2007a). Thirty-one flavors of *Drosophila* rab proteins. Genetics 176, 1307–1322.
Zhang X, He X, Fu XY, Chang Z (2006). Varp is a Rab21 guanine nucleotide exchange factor and regulates endosome dynamics. J Cell Sci 119, 1053–1062.
Zhang Y *et al.* (2007b). Loss of Vac14, a regulator of the signaling lipid phosphatidylinositol 3,5-bisphosphate, results in neurodegeneration in mice. Proc Natl Acad Sci USA 104, 17518–17523.
Zhu H, Zhu G, Liu J, Liang Z, Zhang XC, Li G (2007). Rabaptin-5-independent membrane targeting and Rab5 activation by Rabex-5 in the cell. Mol Biol Cell 18, 4119–4128.